Geological Magazine

www.cambridge.org/geo

Original Article

Cite this article: Spry PG, Mathur RD, Teale GS, and Godfrey LV (2022) Zinc, sulfur and cadmium isotopes and Zn/Cd ratios as indicators of the origin of the supergiant Broken Hill Pb–Zn–Ag deposit and other Broken Hill-type deposits, New South Wales, Australia. *Geological Magazine* **159**: 1787–1808. https://doi.org/10.1017/S0016756822000590

Received: 24 March 2022
Revised: 16 May 2022
Accepted: 23 May 2022
First published online: 20 July 2022

Keywords:
Zn, Cd and S isotopes; Broken Hill Pb–Zn–Ag deposit; granulite facies; Zn/Cd ratios of sphalerite

Author for correspondence:
Paul G. Spry, Email: pgspry@iastate.edu

Zinc, sulfur and cadmium isotopes and Zn/Cd ratios as indicators of the origin of the supergiant Broken Hill Pb–Zn–Ag deposit and other Broken Hill-type deposits, New South Wales, Australia

Paul G. Spry[1], Ryan D. Mathur[2], Graham S. Teale[3] and Linda V. Godfrey[4]

[1]Department of Geological and Atmospheric Sciences, Iowa State University, 253 Science Hall, Ames, Iowa 50011-1027, USA; [2]Department of Geology, Juniata College, 1700 Moore Street, Huntingdon, Pennsylvania 16652, USA; [3]Teale & Associates Pty Ltd, PO Box 740, North Adelaide, South Australia 5006, Australia and [4]Department of Earth and Planetary Sciences, Rutgers University, Wright-Rieman Laboratories, Busch Campus, 610 Taylor Road, Piscataway, New Jersey 08854-8066, USA

Abstract

Various genetic models have been proposed for the supergiant Proterozoic Broken Hill Pb–Zn–Ag deposit largely based on geological and geochronological evidence. Here we present Zn, Cd and S isotope compositions as well as Zn/Cd ratios of sphalerite from Broken Hill and minor Broken Hill-type deposits (Australia) to help constrain these models but focus on syngenetic and magmatic–hydrothermal processes, since epigenetic models can be rejected because the orebodies were deformed and metamorphosed by the Olarian Orogeny. Values of $\delta^{34}S_{VCDT}$, $\delta^{66}Zn_{AA\text{-}ETH}$ and $\delta^{114}Cd_{NIST\ SRM\ 3108}$ for sphalerite from Broken Hill range from +0.27 to +4.73 ‰, −1.15 to +0.46 ‰ and −0.48 to +0.01 ‰, respectively, while those for the smaller Broken Hill-type deposits range from −5.11 to +1.28 ‰, −0.97 to +0.10 ‰ and −1.02 to +2.59 ‰, respectively. By combining published S isotope data of sulfides from the Broken Hill district with those obtained here, the sources of sulfur via thermochemical sulfate reduction, bacterial sulfate reduction and a magmatic origin cannot be distinguished. However, when the S isotope compositions are considered along with the broad range of Cd and Zn isotope data for sphalerite, which are among the lightest and heaviest yet reported for a sulfide deposit, the isotopic datasets are consistent with low-temperature biogenic processes associated with syngenetic deposition of sulfides. Cadmium isotope compositions when coupled with Zn/Cd ratios of sphalerite have previously been used to classify Pb–Zn deposits, including low-temperature, high-temperature and exhalative ores. However, the Zn/Cd ratios of sphalerite from Broken Hill cannot be used for such classification purposes.

1. Introduction

The Broken Hill Pb–Zn–Ag deposit (280 Mt of 10.0 % Pb, 8.5 % Zn and 148 g/t Ag; Huston *et al.* 2006) is the world's largest massive sulfide deposit. It occurs in the southern Curnamona province, New South Wales (Australia), along with hundreds of minor Broken Hill-type (BHT) deposits. They are hosted in the Palaeoproterozoic Willyama Supergroup in an ~7 km thick package of multi-deformed and metamorphosed clastic sediments, bimodal (felsic and mafic) volcanic and volcaniclastic rocks, chemical sediments and granitoids (Fig. 1) (Willis *et al.* 1983; Burton, 1994). Metamorphic conditions reached granulite facies. Given the high metamorphic grade and extreme deformation, which have largely removed primary textures in the ore, a variety of origins have been proposed for the formation of the deposit. These ore deposit models are summarized in Greenfield (2003) and include: (1) syngenesis in which the deposit was considered to have formed by submarine exhalative/inhalative processes (Plimer, 1979; Wright *et al.* 1987; Parr & Plimer, 1993); (2) syntectonic (Katz, 1976; Findlay, 1994; Nutman & Ehlers, 1998); (3) post-tectonic (Andrews, 1922; Williams *et al.* 1996); (4) magmatic–hydrothermal (Crawford & Maas, 2009); and (5) partial melting (Mavrogenes *et al.* 2001; Frost *et al.* 2011).

In attempting to add clarity to how the Broken Hill deposit formed, we evaluate sulfur, zinc and cadmium isotopes of sphalerite along with the Zn/Cd ratios of sphalerite. Although various zinc isotopic studies have been conducted on several types of ore deposits including, Mississippi Valley-type Pb–Zn (MVT) (e.g. Pašava *et al.* 2014; Wen *et al.* 2016; Zhu *et al.* 2018, 2021; Li *et al.* 2019), Irish-type Pb–Zn (Wilkinson *et al.* 2005; Gagnevin *et al.* 2012, 2014); volcanogenic massive sulfide (VMS) (Mason *et al.* 2005), sedimentary exhalative (Sedex) (e.g. Kelley *et al.* 2009; Gao *et al.* 2018; Baumgartner *et al.* 2021; Wang *et al.* 2021) and active hydrothermal vents (e.g. John *et al.* 2008), Zn isotope studies of sphalerite in regionally metamorphosed ore deposits are

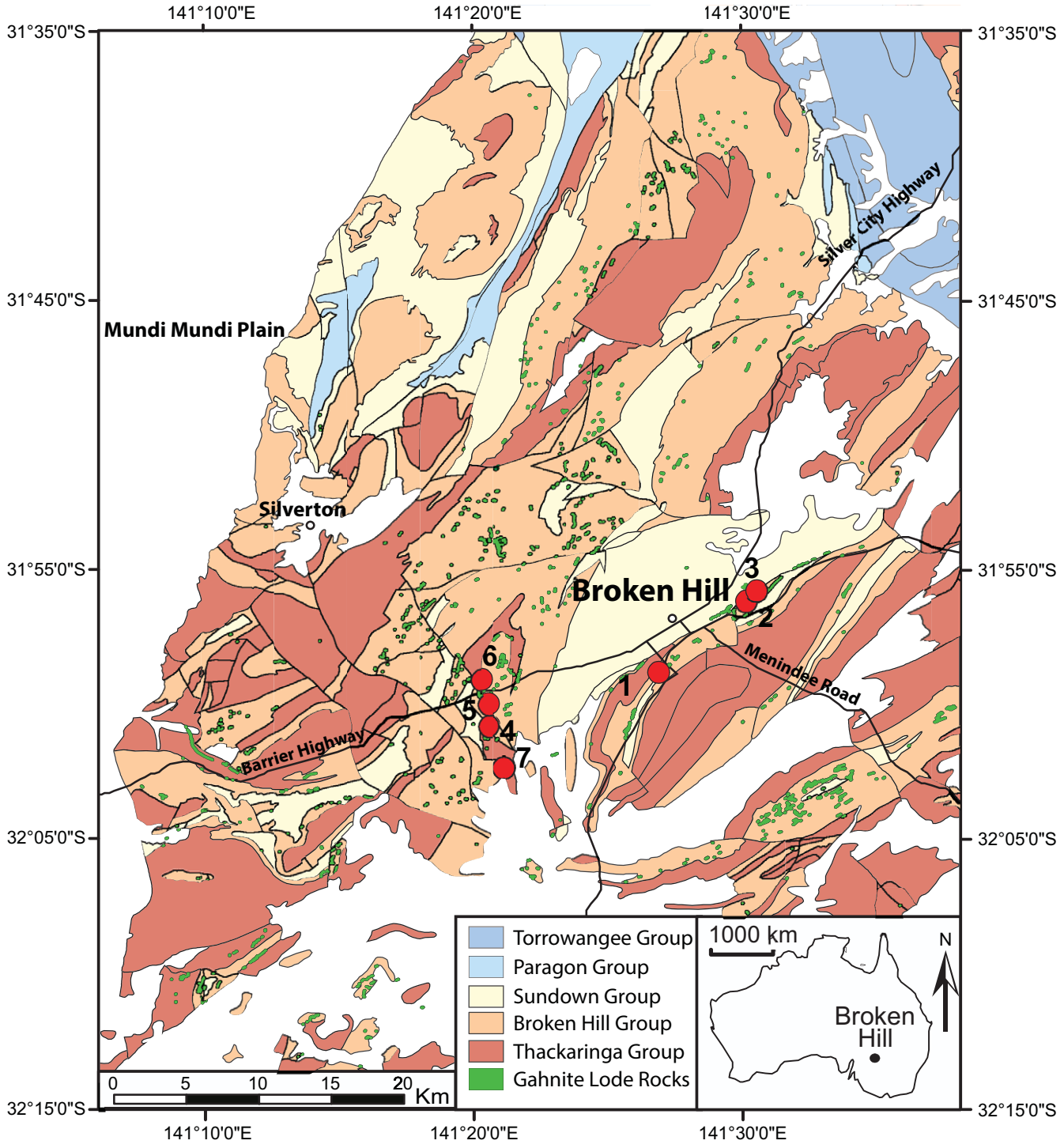

Fig. 1. (Colour online) Geological map of the southern Curnamona Province and study sites: 1 – Broken Hill; 2 – Flying Doctor; 3 – Globe; 4 – Henry George; 5 – Esmeralda; 6 – 11:30; 7 – Pinnacles (modified after Laing *et al.* 1978; Page *et al.* 2005; O'Brien *et al.* 2015).

restricted to those of Matt *et al.* (2020, 2022) on sphalerite and zinc oxides (zincite and franklinite) from the carbonate- and evaporate-hosted Balmat Zn deposit (New York) and the marble-hosted Franklin Zn deposit, New Jersey. A preliminary Zn isotope study was also made on sphalerite from the Gamsberg Sedex Zn deposit (South Africa) by S. E. Foulkes (unpub. M.Sc. thesis, Rhodes Univ., 2014), which, along with the Balmat deposit, was metamorphosed to the amphibolite facies. The Franklin district mines, like the Broken Hill district, were metamorphosed to the granulite facies. Although not part of this study, the Zn isotope composition of galena from various unmetamorphosed Chinese Pb–Zn deposits were obtained by Wang *et al.* (2020, 2021).

Cadmium isotopes have been used to evaluate the source of Cd in rocks, ore deposits, unconsolidated sediments, seawater, meteorites and biological samples (e.g. Wohmbacher *et al.* 2003, 2004; Lacan *et al.* 2006; Zhu *et al.* 2016, 2021; Hohl *et al.* 2017), and to

https://doi.org/10.1017/S0016756822000590 Published online by Cambridge University Press

understand geochemical processes. Wen *et al.* (2016) suggested that Cd isotope compositions of sphalerite when coupled with Zn/Cd ratios of sphalerite can be used to classify Pb–Zn deposits. They identified three classes of ore systems: high-temperature (i.e. skarn, VMS, porphyry, magmatic–hydrothermal), low-temperature (i.e. MVT) and exhalative (i.e. Sedex, seafloor hydrothermal). To date, no Cd isotope study has been done on an ore deposit subject to regional metamorphism. The criteria for deposit classification as applied by Wen *et al.* (2016) is discussed further in Section 5.b.

Several sulfur isotope studies have been conducted on sulfides from Broken Hill and the smaller BHT deposits (Lawrence & Rafter, 1962; Stanton & Rafter, 1966, 1967; Both & Smith, 1975; Dong *et al.* 1987; Spry, 1987; Parr, 1992, 1994*a*; Huston *et al.* 1995), while the major-element composition of sphalerite was determined by, for example, Both (1973), Hodgson (1975) and Lockington *et al.* (2014). Trace-element compositions of sphalerite are largely restricted to the studies of Both (1973) and Lockington *et al.* (2014). Both (1973) determined the trace-element content (including Cd) of sphalerite separates from each orebody using X-ray fluorescence spectrographic techniques, while Lockington *et al.* (2014) analysed two samples of sphalerite using a laser ablation inductively coupled plasma mass spectrometer. We have obtained new major- and trace-element compositions of sphalerite because individual sphalerite compositions were not provided by Both (1973) and Hodgson (1975) and only two samples were obtained by Lockington *et al.* (2014). Both (1973) plotted the compositions to show the ranges of Cd in sphalerite for each orebody, which is unusable for our purposes, while Hodgson (1975) analysed Zn, Mn, Fe and S but not Cd. The new sphalerite compositions obtained here, along with Cd isotope analyses from the Broken Hill deposit, are used to evaluate the origin of the Broken Hill deposit given the classification scheme of Wen *et al.* (2016). These geochemical parameters along with Zn isotope composition of sphalerite have not previously been applied to lead–zinc–silver mineralization in the Broken Hill district. The study of Zn isotopes of sphalerite from Broken Hill is particularly relevant given the partial melt model of Mavrogenes *et al.* (2001) and Frost *et al.* (2011) for the formation of the deposit, which was recently applied to the metamorphosed Balmat deposit by Matt *et al.*, 2020) to explain the fractionation of Zn isotopes in some orebodies. The aim of the study is to utilize Zn, Cd and S isotopes and the Zn/Cd ratios of sphalerite to shed light on the controversy surrounding the origin of the Broken Hill deposit and minor BHT deposits in the Broken Hill district.

2. Geological setting

Depositional ages of the Willyama Supergroup are ~1720–1640 Ma, with the Broken Hill Group, which hosts the Broken Hill deposit, having formed at ~1695–1685 Ma (Page & Laing, 1992; Page *et al.* 2005) (Fig. 2). Metamorphic conditions in and adjacent to the Broken Hill deposit were ~700–800 °C and 5–6 kbar (Phillips & Wall, 1981; Powell & Downes, 1990; White *et al.* 2004) but decreased to the amphibolite facies in the northern part of the Willyama Domain. The minor BHT deposits studied here (11:30, Flying Doctor, Esmeralda, Henry George, Globe, Pinnacles) were all subjected to the granulite facies. The deposits were intensely deformed and affected by at least three periods of deformation. Two of these deformational episodes resulted in the Broken Hill deposit being subject to two isoclinal fold events (Laing *et al.* 1978; Willis *et al.* 1983) with the structural data of Laing *et al.* (1978) suggesting that the deposit and the contained orebodies were overturned. The Broken Hill deposit is 8 km long and consists of at least six separate orebodies (from stratigraphic bottom to the top, they are C, B and A lodes and 1, 2 and 3 lenses; Figs 3, 4) each of which has a characteristic gangue mineralogy and metal ratio. Details of the vast array of minerals (>350) found in the Broken Hill deposit are given in Plimer (1984) and Birch (1999). The main metallic minerals consist of sphalerite and galena, with minor amounts of pyrrhotite, chalcopyrite, arsenopyrite, löllingite, tetrahedrite and various sulfosalts. The most abundant silver-bearing minerals are galena and tetrahedrite with pyrargyrite, polybasite, stephanite, argentite, antimonial silver, allargentum, dyscrasite, argentopyrite and native silver occurring in lesser amounts (Lawrence, 1968; Both & Stumpfl, 1987). The dominant gangue minerals in each orebody are rhodonite, fluorite, quartz (3 lens), calcite, rhodonite, wollastonite (2 lens), quartz, calcite, wollastonite (1 lens), rhodonite, manganoan hedenbergite (A lode), quartz (B lode) and quartz (C lode). Based, in part, on Laing *et al*'s (1978) assumption that the deposit was structurally overturned, Groves *et al.* (2008) identified a feeder zone system in the C lode, with cross-cutting blue quartz-gahnite ± garnet rocks serving as the metamorphosed alteration zone. However, some workers (e.g. Mavrogenes *et al.* 2001; Webster, 2006; Frost *et al.* 2011) suggested that the deposit was not overturned so that the orebodies are the correct way up with 3 lens being at the stratigraphic base of the deposit and C lode at the top. The C, B and A lodes and 1 lens are characterized by Zn > Pb, whereas the 2 and 3 lenses have Pb ≥ Zn. By invoking major partial melting of the deposit, Mavrogenes *et al.* (2001) and Frost *et al.* (2011) argued that the zinc lodes (i.e. A, B and C lodes and 1 lens) are restites of Pb-rich sulfide melts implying that these melts migrated through the stratigraphy to form the Pb-rich orebodies (i.e. 2 and 3 lenses).

The Broken Hill deposit is intimately associated with a package of rocks that Johnson & Klingner (1975) referred to as the 'lode horizon', which consists of quartz garnetite, garnetite, blue quartz and blue quartz-gahnite rocks, and 'lode' pegmatite (Spry & Wonder, 1989; O'Brien *et al.* 2015). Apart from metasedimentary rocks, blue quartz-gahnite rocks and quartz garnetite are the two most common rock types spatially associated with minor BHT deposits (Barnes *et al.* 1983). A summary of the geological setting for the deposits from which samples were analysed is given in Table 1.

3. Samples and analytical methods

3.a. Cadmium and zinc isotopes

Thirty-one samples were collected from drill core and from underground locations at the Broken Hill and Pinnacles deposits. Some of the samples were used previously in the studies of Spry & Wonder (1989) and O'Brien *et al.* (2015). Approximately 50 mg of sphalerite powder was dissolved in 4 ml of ultrapure heated (80 °C) aqua regia for 8 hours. Complete dissolution was visually confirmed. The solution was cut into two equal aliquots and used for chromatographic separation. The procedure for the preparation of the Cd and Zn isotopes is identical to that given by Wang *et al.* (2020, 2021). All reported results show mass dependence.

The Cd isotopic compositions were measured on a Neptune multicollector inductively coupled plasma mass spectrometer (MS-ICP-MS) at Rutgers University. Cadmium was purified using the anion exchange chromatograph (Cloquet *et al.* 2005) with

https://doi.org/10.1017/S0016756822000590 Published online by Cambridge University Press

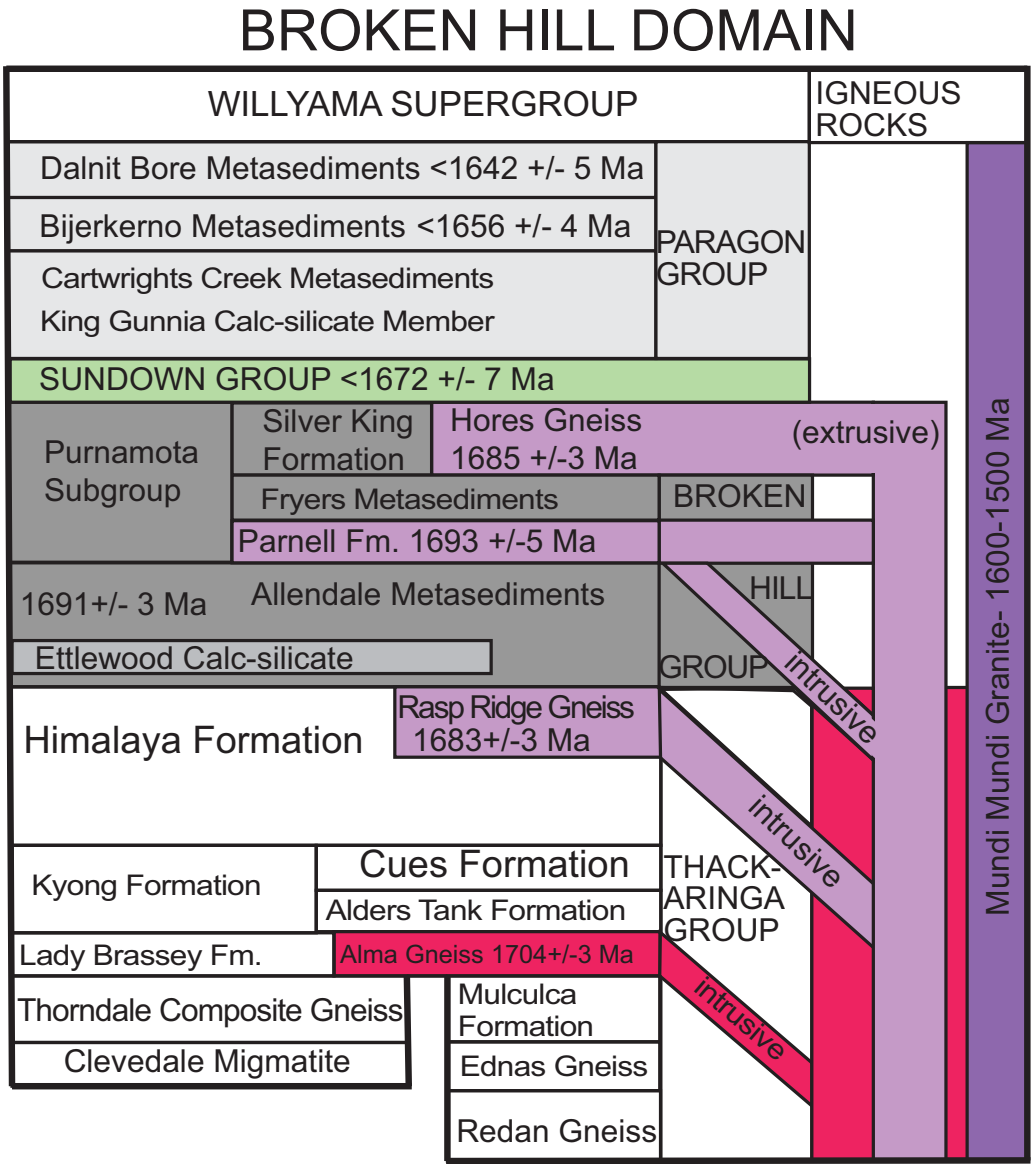

Fig. 2. (Colour online) Stratigraphic column and ages of rocks in the Broken Hill domain (after Conor & Preiss, 2008). The Broken Hill and BHT deposits occur in the Hores Gneiss of the Purnamota Subgroup, while the Pinnacles deposit likely occurs in the Cues Formation stratigraphically lower in the Broken Hill domain.

volumetric yields for the samples greater than 94 % after two rounds of column chromatography. Yield checks were measured on an Agilent 5900 ICP-optical emission spectrometer (ICP-OES) at Juniata College. Zinc and Cd concentrations were determined with standard calibration curves that ranged from 0.5 to 20 ppm, and yttrium was used as an internal standard for analysis.

The chromatography for Cd involved 2 ml of wet BioRad AG MP-1 resin chloride form (100–200 mesh), which was added to a 10 ml BioRad chromatography column. The resin was sequentially cleaned with 10 ml of 2 % HNO_3, 10 ml of MQ water (18.2 W) and 5 ml of 1.2 molar HCl. The sample was loaded onto the resin with 1 ml of 1.2 molar HCl and the unwanted ions were sequentially eluted with lower molality HCl and the Cd was collected in 17 ml of 0.0012 molar HCL. This process was repeated with the use of new resin for the second column to eliminate Sn. The chromatography was effective, as no ^{115}Sn voltages were recorded above the 2 mV background. The ^{115}Sn mass was monitored in H4 cup, with ^{107}Ag in L4 cup, ^{109}Ag in L2 cup, ^{110}Cd in L1 cup, ^{111}Cd in Ax cup, ^{112}Cd in H1 cup, ^{113}Cd in H2 cup, ^{114}Cd in H3 cup and ^{115}Sn in H4 cup. Instrumentation setup and introduction was similar to that of Wasylenki *et al.* (2014). All samples were doped with 150 ppb NIST 987 Ag isotope standard, which was used to correct for mass bias using the exponential fractionation correction (Maréchal *et al.* 1999). The ^{107}Ag/^{109}Ag of the NIST 987 Ag isotope standard is reported as 1.07638. Solutions were measured at 200 ppb Cd, with on-peak blank subtraction in one block of 30 ratios. The reported values are an average of two separate measurements, and the data are presented relative to the NIST SRM 3108 Cd standard in per mil notation defined as: $\delta^{114/110}$Cd (‰) = $((^{114}Cd/^{110}Cd)_{sample}/(^{114}Cd/^{110}Cd)_{NIST\ SRM\ 3108} - 1) \times 1000$ (Abouchami *et al.* 2013). All data cited here from the literature are converted relative to the NIST SRM 3108 standard ($\delta^{114}Cd_{NIST\ SRM\ 3108} = \delta^{114}Cd_{Nancy\ SPEX} - 0.11$ ‰; Xu *et al.* 2020).

Measured errors of ratios were in the fifth or sixth decimal and do not represent a conservative estimation of error. Errors for the measured values are constrained in two ways. The variation of NIST SRM 3108 throughout the measuring session was 0.05 ‰ (2s, $n = 27$). The second means for error estimation was by measuring a High Purity Standard ICP-MS standard during the two sessions. The value of the standard is $\delta^{114}Cd = -0.53$ ‰ ± 0.06 (2s,

https://doi.org/10.1017/S0016756822000590 Published online by Cambridge University Press

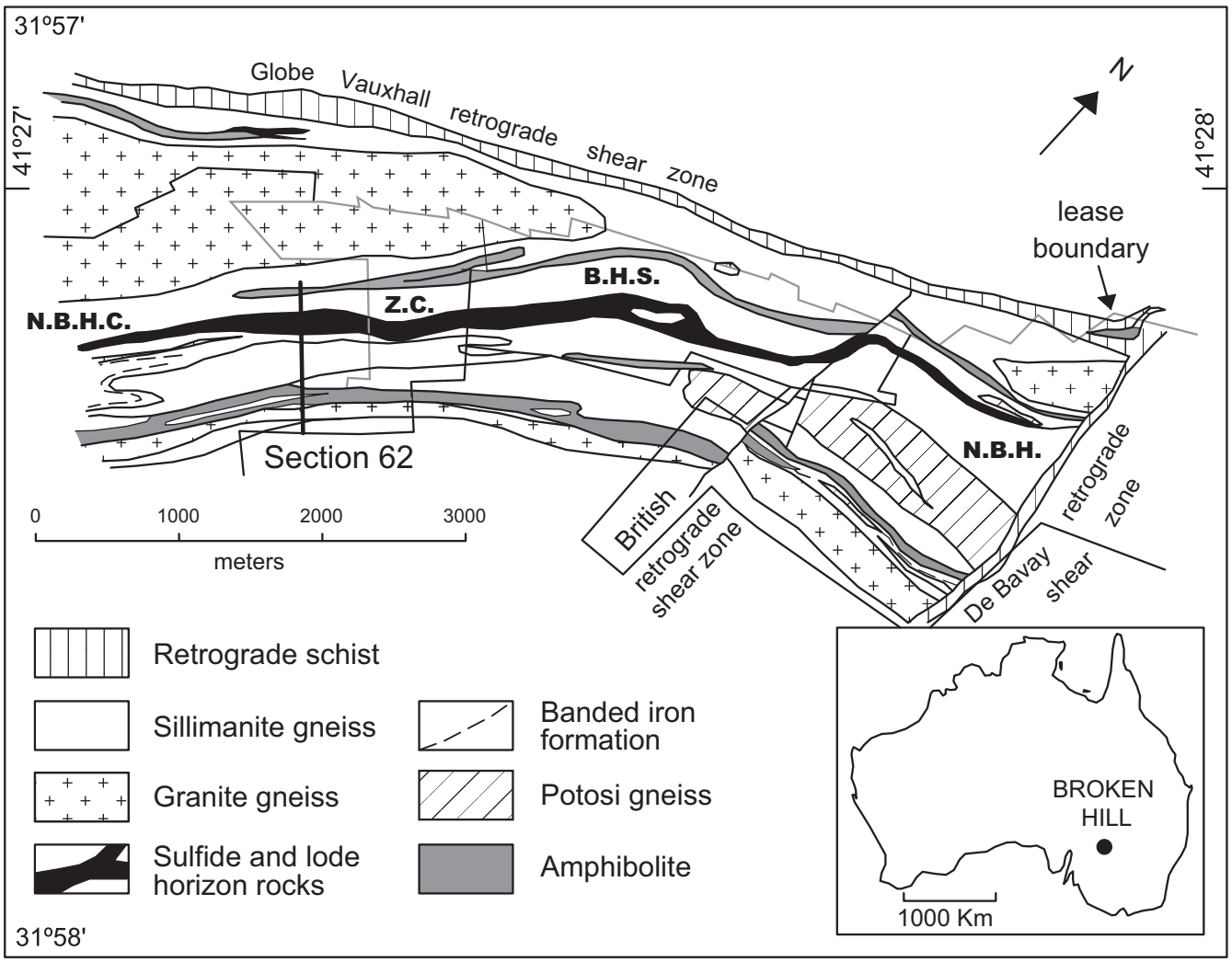

Fig. 3. Geological map of the Broken Hill deposit. Abbreviations: N.B.H.C – New Broken Hill Consolidated mine (currently part of Southern Operations operated by Perilya Broken Hill Limited); Z.C. – Zinc Corporation mine (currently part of Southern Operations operated by Perilya Broken Hill Limited); B.H.S. – Broken Hill South mine; N.B.H. – North Broken Hill mine (currently North mine operated by Perilya Broken Hill Limited). Cross-section No. 62 is shown as a bold black line (see Fig. 4 for cross-section).

$n = 10$) and is considered the error of measurements. All duplicate measurements fall within reported errors.

The chromatography for Zn also involved the BioRad MP-1 anion exchange resin using the protocol defined by Maréchal *et al.* (1999). Yields from the columns were tested volumetrically and were all greater than 95 %. The mass bias corrections for Zn using Cu (NIST 976) were employed for these samples and then the corrected values were bracketed by the standards (Archer & Vance, 2004; Chapman *et al.* 2004, 2006; Peel *et al.* 2008). Solutions were measured at 150 ppb Cu and 200 ppb Zn ($^{63}Cu = 7V$ and $^{66}Zn = 4V$). One block was 30 ratios in the analytical session, and the Zn isotope values are reported in traditional per mil notation relative to the AA–ETH standard: $\delta^{66}Zn$ (‰) = $((^{66}Zn/^{64}Zn)_{sample}/(^{66}Zn/^{64}Zn)_{AA-ETH} - 1) \times 1000$. All the data cited here from the literature were converted relative to the AA–ETH standard ($\delta^{66}Zn_{AA-ETH} = \delta^{66}Zn_{JMC3-0749L} - 0.28$ ‰; Archer *et al.* 2017).

Errors for Zn isotopes are calculated in a similar manner to that discussed above for Cd isotopes. Throughout the analytical sessions, the reference material AA–ETH standard compared with itself ($n = 14$) yielded two standard deviations of 0.06 ‰ (2σ) for $\delta^{66}Zn$, which is larger than the error for each sample during the run. The value of USGS BVHO-2 $\delta^{66}Zn_{AA-ETH}$ is +0.02 ‰ ± 0.04 (2s, $n = 3$). The largest error between the two methods is that of the variation of the standard in comparison to itself and is considered the error for reported samples.

3.b. Sulfur isotopes

Sphalerite was separated from ore samples by hand picking under a binocular microscope or was drilled out with a Dremel tool with a 1 mm drill tip. We followed the procedure for sulfur isotope analysis as described by Grassineau (2006). Sphalerite was pulverized in an agate mortar to a powder (1.5 mg), which was then loaded into tin capsules and burned using a Thermo Scientific Flash IRMS IsoLInk elemental analyser. The Sn capsules oxidized at ~1020 °C, and when oxygen was added it flash combusted at 1800 °C (Grassineau, 2006). The oxygen was added at a rate of 300 ml/minute for three seconds. The SO_2 gas produced was purified through a gas chromatography column and then introduced via a Conflo IV Universal Interface system into a continuous flow-type dual-inlet Thermo Scientific Delta V Series Isotope Ratio mass

https://doi.org/10.1017/S0016756822000590 Published online by Cambridge University Press

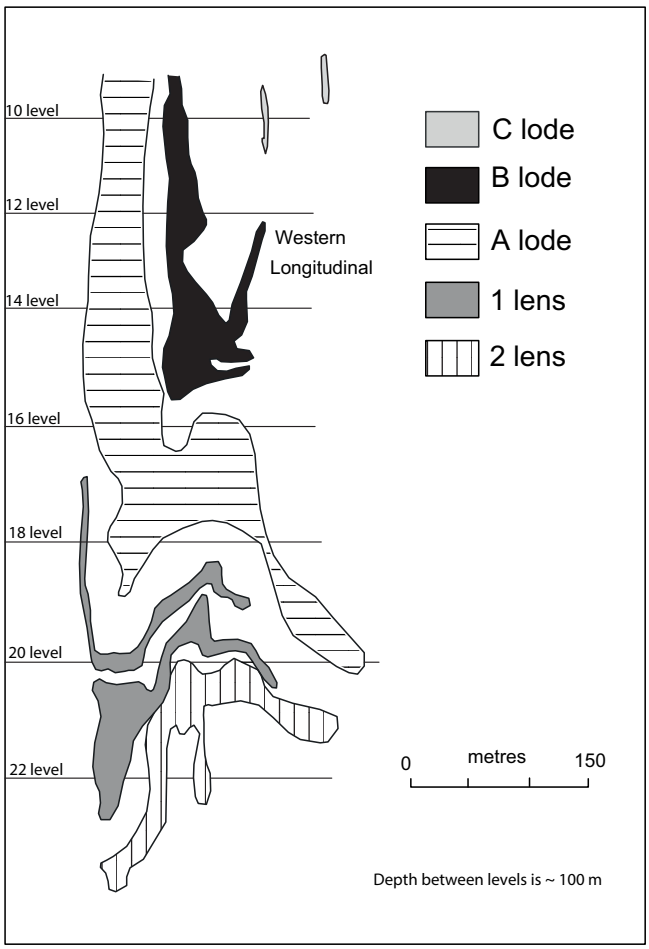

Fig. 4. Cross-section (No. 62) through the New Broken Hill Consolidated mine haulage shaft, looking south l8 degrees east, Broken Hill deposit. Note that the orebodies are structurally overturned with C lode occurring at the stratigraphic base of the deposit. The 3 lens orebody is not shown here as it only occurs in the central and northern parts of the deposit, where it occurs at the stratigraphic top. The figure has been modified after Pratten (1965).

spectrometer under He flow. The analysis time was ~420 seconds. The $\delta^{34}S_{VCDT}$ values were calculated using calibration curves obtained for the following standards, some of which were obtained from the Queen's Facility for Isotope Research (QFIR), Queen's University, Canada: NBS 127 barite = +20.3 ‰ (±0.3 ‰), IAEA-SO-6 barite = −34.1 ‰, QFIR pyrite = −0.5 ‰, IAEA-SO-5 barite = +0.5 ‰, MRC pyrite = +0.7 ‰, Q-GEMA pyrite = +3.0 ‰, M6801 barite = +12.5 ‰, and two internal standards provided by Thermo Scientific: peat = −13.15 ‰ (±0.3 ‰) and sulfanilimide = −1.24 ‰ (±0.2 ‰). These values are relative to the internationally recognized sulfur isotope standard Cañon Diablo troilite (FeS). The analytical precision of the data is ±0.1 ‰.

3.c. Major- and trace-element composition of sphalerite

Part of the dissolved separates of sphalerite in solution that were analysed for Zn and Cd isotopes from the Broken Hill deposit as well as smaller BHT deposits (11:30, Esmeralda, Flying Doctor, Henry George) were also analysed for Ag, Cd, Cu, Fe and Zn using an Agilent 5900 ICP-OES at Juniata College. Quantitative analyses of sphalerite were also performed on a JEOL JXA-8530FPlus electron microprobe at the University of Minnesota. Analytical conditions for determining sphalerite compositions used an accelerating voltage of 15 kV, beam current of 50 nA and a beam diameter of 5 microns. Elements were acquired using analysing crystals LIFL for Zn kα, Mn kα, Fe kα and Cu kα, PETL for Cd lα, and PETJ for S kα and Ag lα. The standards were Mn-olivine and synthetic Mn_2SiO_4 for Mn, Cu metal for Cu, pyrite for Fe, sphalerite for Zn and S, hessite for Ag and cadmium sulfide (CdS) for Cd. The on-peak counting time was 10 seconds for Zn kα, Mn kα, Fe kα, Cu kα and S kα, 40 seconds for Ag lα and 60 seconds for Cd lα. The mean atomic number (MAN) background intensity method was used instead of the traditional off-peak background acquisition (Donovan & Tingle, 1996; Donovan *et al.* 2016). The MAN background intensity data was calibrated and continuum absorption corrected for Cd lα, Zn kα, Mn kα, Fe kα, Cu kα, S kα and Ag lα. Unknown and standard intensities were corrected for dead-time. The Phi-Rho-Z matrix correction algorithm Armstrong/Love Scott (CitZAF) was used along with the mass absorption coefficients dataset FFAST (Chantler *et al.* 2005).

4. Results

4.a. Sulfur isotopes

Sulfur isotope compositions of 31 samples of sphalerite are in Table 2. The values of $\delta^{34}S$ from Broken Hill range from +0.27 to +4.73 ‰ ($n = 19$), while those for the following smaller BHT deposits are: Pinnacles (−3.08 to −0.94 ‰, $n = 3$), Esmeralda (+1.24 to +1.28 ‰, $n = 2$), Henry George (−1.06 to +1.17 ‰, $n = 4$), 11:30 (−5.11 ‰, $n = 2$) and Flying Doctor (−0.36 ‰, $n = 1$) (Fig. 5). Sulfur isotope compositions of sulfides from these minor deposits had not previously been obtained, except for the Pinnacles deposit, the second largest Pb–Zn–Ag deposit in the Willyama Domain, where Parr (1992, 1994*a*) reported a range of $\delta^{34}S$ = −3.5 to +3.7 ‰. Other sulfur isotope studies of sulfides from the Broken Hill area include analyses of sphalerite, galena, pyrrhotite and chalcopyrite. Both & Smith (1975) recorded $\delta^{34}S$ values of between −2.1 and +2.4 ‰ per mil and between −3.8 and +5.4 ‰ for sulfides from the main Broken Hill lode and 26 minor BHT deposits (including Pinnacles), respectively, while Spry (1987) showed a broader isotopic range for the Broken Hill deposit of −3.3 to +6.7 ‰. The isotopic compositions obtained by Lawrence & Rafter (1962; $\delta^{34}S$ = +0.4 to +1.7 ‰) and Stanton & Rafter (1966; $\delta^{34}S$ = −2.2 to +4.7 ‰, 1967; $\delta^{34}S$ = −1.5 to +2.8 ‰) for Broken Hill fall within the range given by Spry (1987).

By combining the S isotope data for sphalerite, galena, pyrrhotite and chalcopyrite of Both & Smith (1975) and Spry (1987), the latter proposed that there may be a weak increase in isotopic values from the stratigraphic footwall (C lode) through to the hanging wall (3 lens). However, by adding the S isotope data for sphalerite obtained here with these two studies it is apparent that there is no systematic increase from the footwall to the hanging wall. Instead, there is an increase in the average isotopic compositions for sphalerite in C lode ($\delta^{34}S = 0$ ‰) to the top of the Zn lodes (i.e. 1 lens; $\delta^{34}S$ = +2.2 ‰) with a slight decrease to 1 ‰ in 3 lens (Fig. 6a). Although galena was not analysed here, the combined data of Both & Smith (1975) and Spry (1987) show a steady increase in the average $\delta^{34}S$ galena composition from C lode (−1.4 ‰) to 2 lens (+1.3 ‰) and 3 lens (+1.2 ‰). Data for the Zn mineralization from the North mine is shown in Figure 6a but was not included owing to uncertainty in its stratigraphic position (possibly 1 lens or

https://doi.org/10.1017/S0016756822000590 Published online by Cambridge University Press

Table 1. Summary of geological characteristics of Broken Hill and BHT deposits (modified after O'Brien *et al*. 2015)

Deposit: Lat., Long.	Grade, drilling data, tonnage*, metallic minerals†	Gangue minerals	Lode and country rocks	References
Broken Hill −31.982244, 141.450679	300 Mt of 10.0 % Pb, 8.5 % Zn, 0.14 % Cu and 148 g/t Ag: Gn–Sp–Ccp ± Asp ± Po ± Lo	Qz–Ghn–Rhd–Grt ± Ms ± Sil ± Amp ± Ap ± Fsp	Qz–Grt and Qz–Ghn rocks envelope orebodies in psammitic–psammopelitic–pelitic metasediments (Hores Gneiss) and quartzofeldspathic gneiss (Potosi Gneiss); Ghn–Qz ± Grt rocks are most abundant in the structural hanging wall, spatially associated with BIF	Johnson & Klingner (1975); Parr & Plimer (1993); Webster (2006)
11:30 (BHT) −31.997688, 141.350647	0.2 Mt @ 1 % Pb, 12 % Zn, 7 g/t Ag; Sp ± Py ± Po ± Asp ± Gn	Ghn–Qz–Grt–Bt ± Fsp	Qz–Ghn–Grt lode rocks in psammite–psammopelitic metasediment (Broken Hill Group) occur between two plagioclase gneiss units; locally intersected by a mafic amphibolite	Perilya (2008); O'Brien *et al.* (2015)
Esmeralda (BHT) −32.01528, 141.34667	Unknown tonnage, 5–7 % Pb + Zn (up to 5 m drill intersection); Sp ± Po ± Py	Qz-Cal-Pmt-Wo-Grt-Mag	Qz–Cal lode rocks in psammite–psammopelitic metasediment (lower Broken Hill Group) and is also associated with amphibolites, calc-silicate units and rare Potosi Gneiss	Heimann *et al.* (2013); D. Rogers (pers. comm. 2022)
Flying Doctor (BHT) −31.917398, 141.524643	1.5 Mt @ 4 % Pb, 3 % Zn, 44g/t Ag; Gn–Sp–Asp–Po ± Ccp ± Py	Qz–Ghn ± Grt ± Bt ± Chl ± Ap	Qz–Ghn–sulphide ± Grt lode rock in pelitic to psammopelitic metasediments (Broken Hill Group)	Burton (1994); Teale *et al.* (2006)
Globe (BHT) −31.910304, 141.542916	2686 t produced, with 502 kg Ag and 512 t Pb recorded; Cer–Gn–Sp ± Mlc ± Po	Fsp–Qz ± Chl ± Ms ± Grt ± Tur	Qz–Ghn lode rock in pelitic–psammitic metasediments (Purnamoota Subgroup) and Potosi Gneiss	Burton (1994)
Henry George (BHT) −32.030166, 141.350771	1.3 Mt @ 1 % Pb, 8 % Zn, 14 g/t Ag; Sp–Po–Py–Gn ± Asp	Qz–Ghn–Fsp–Bt ± Grt	Qz–Ghn lode rock in pelitic to psammopelitic metasediment with minor pegmatitic segregations (Broken Hill group). Lode rocks occur adjacent to amphibolite and ultramafic dyke	Perilya (2008)
North Mine Zinc Lode −31.9142, 141.5384	Also known as the 'Fitzpatrick Zinc Lode'. Past production 0.04 Mt @ 9.6 % Zn, 4.6 % Pb, 187 g/t Ag; reserves: 1 Mt @ 9.0 % Pb, 7.0 % Zn, 140 g/t Ag: Sp–Po ± Gn ± Py ± Ccp	Qz–Grt–Ghn ± Sil ± Bt	Po–Sp-bearing Grt–Qz lode rocks bounded by Grt–Sil-bearing psammites–psammopelites and pelitic metasediments	Widdop (1983); Webster (2006)
Pinnacles (BHT) −32.052049, 141.328716	Second largest Broken Hill deposit. 2 Mt @ 6–11 wt % Pb, 2.5 wt % Zn, 300–500 g/t Ag; Gn–Sp–Py–Sp ± Asp ± Lo ± Ttr ± Po	Fsp–Ghn–Amp–Grt–Mag–Qz–Ghn ± Bt ± Ms	Three sulfide-bearing lode (two Pb and one Zn) with associated Qz–Ghn and Qz–Grt lode rock occur in pelitic and psammitic metasediment (Cues Formation)	Parr (1994*a*)

*Estimates of grades and tonnage supplied by Perilya Ltd for North Mine Zinc Lode, Henry George and 11:30.
†Mineral abbreviations after Whitney & Evans (2010); Amp – amphibole; Ap – apatite; Asp – arsenopyrite; Az – azurite; Bt – biotite; BHT – Broken Hill-type; BIF – banded iron formation; Cal - calcite; Cer – cerussite; Ccp – chalcopyrite; Chl – chlorite; Di – diopside; Fsp – feldspar; Ghn – gahnite; Gn – galena; Grt – garnet; Lo – löllingite; Mag – magnetite; Mlc – malachite; Ms – muscovite; Pmt - piemontite; Po – pyrrhotite; Py – pyrite; Rhd – rhodonite; Qz – quartz; Sil – sillimanite; Sp – sphalerite; Ttr – tetrahedrite; Tur – tourmaline; Wo – wollastonite.

Table 2. Zn, Cd and S isotope data and major–trace-element contents of sphalerite (ppm) from Broken Hill and minor BHT deposits

Sample no.	Deposit	Ore body	Location or drill core	$\delta^{34}S$ ‰	$\delta^{66}Zn$ ‰	$\delta^{114}Cd$ ‰	Ag	Cd	Cu	Fe	Zn	Zn/Cd
BH-1	Broken Hill	3 lens	Blackwoods pit	2.02	−1.15	−0.23	2842	2769	4255	83768	607189	219
BH-2	Broken Hill	3 lens	North mine	0.27	0.04	−0.14	386	2439	545	75201	1024854	420
GT-1	Broken Hill	3 lens	North mine 37 level	0.66	0.04	−0.04	155	10345	151369	769324	3040252	294
532-502	Broken Hill	3 lens	North mine garnet rim	1.83	−0.35	−0.25	70	3060	16818	142770	1131631	370
6542 92.1 m	Broken Hill	3 lens	North mine	2.17	−0.08	−0.44	403	2381	2063	155596	780859	328
Z3590 66.9 m	Broken Hill	2 lens		1.22	−0.09	0.01	581	2451	10266	162487	915607	374
532-331	Broken Hill	1 lens		4.73								
Z3590 0.6 m	Broken Hill	A lode		2.20	−0.04	−0.36	144	10882	16083	937588	3050190	280
Z3590 15.6	Broken Hill	A lode		4.47	0.46	−0.08	32	181	1145	286924	214846	1189
7254 88.7 m	Broken Hill	A lode		1.66	−0.07	−0.48	156	7882	45109	841379	2433570	309
7318 100.5 m	Broken Hill	A lode		2.24	−0.39	−0.12	17	2529	0	326292	1167979	462
6303 6.2 m	Broken Hill	SA lode		1.29	0.30	−0.23	17	1435	11284	170209	784061	546
JB-10-82	Broken Hill	Zinc lode	North mine	1.07	−0.02	−0.35	343	3232	7195	234246	1034944	320
JB-10-83	Broken Hill	Zinc lode	North mine, 10783 281 m	1.22	0.08	−0.33	18	5322	474	265437	1203836	226
JB-10-87	Broken Hill	Zinc lode	North mine, 10783 322 m	1.54	−0.77	−0.12	324	2284	3619	245641	1001814	439
6220 20.0 m	Broken Hill	C lode	NBHC	1.48	−0.22	−0.26	790	574	469	146801	383575	668
532-299	Broken Hill	C lode	NBHC	0.98	0.22		17	2656	2246	244523	815529	307
532-300	Broken Hill	C lode	NBHC	1.38	0.25	−0.04	77	2242	1353	234689	682008	304
532-302	Broken Hill	C lode	NBHC	1.66	0.03	−0.24	169	2360	2151	354074	1001871	424
JB-10-52	Esmeralda		PPN133 142.5 m	1.28	−0.76	−0.35	81	2960	1664	222735	908574	307
JB-10-53	Esmeralda		PPN133 143.1 m	1.24	−0.97	−0.03	18	2123	2928	263498	995789	469
JB-10-100	Flying Doctor		3538 39.3 m	−0.36	0.10	−0.77	196	4100	2684	331625	916657	224
JB-10-X	Henry George		PPN94 295 m	−0.24	−0.24	−0.28	412	1950	2464	147419	865877	444
JB-10-23	Henry George		PPN94 295.7 m	−1.06	−0.33	−1.02	29	2210	3563	197197	943294	427
JB-10-27	Henry George		PPN94 300.1 m	0.11	−0.38	−0.15	8	2068	576	188590	1118626	541
JB-10-34	Henry George		PPN95 308.4 m	1.17	−0.25	−0.38	532	1961	592	209415	727040	371
JB-10-43	11:30		PPN106 172.2 m	−5.11	−0.26	−0.04	57	2154	0	190561	933566	433
JB-10-46	11:30		PPN109 208.3 m	−5.11	−0.19	2.59	55	1803	0	173889	935901	519

(*Continued*)

https://doi.org/10.1017/S0016756822000590 Published online by Cambridge University Press

Table 2. (*Continued*)

Sample no.	Deposit	Ore body	Location or drill core	$\delta^{34}S$ ‰	$\delta^{66}Zn$ ‰	$\delta^{114}Cd$ ‰	Ag	Cd	Cu	Fe	Zn	Zn/Cd
BH-109	Pinnacles		Consols Lead lode	−3.08								
BH-113	Pinnacles		2 level	−0.94								
BH-115	Pinnacles		2 level Zinc lode	−1.04								
				±0.14 ‰	±0.09 ‰							

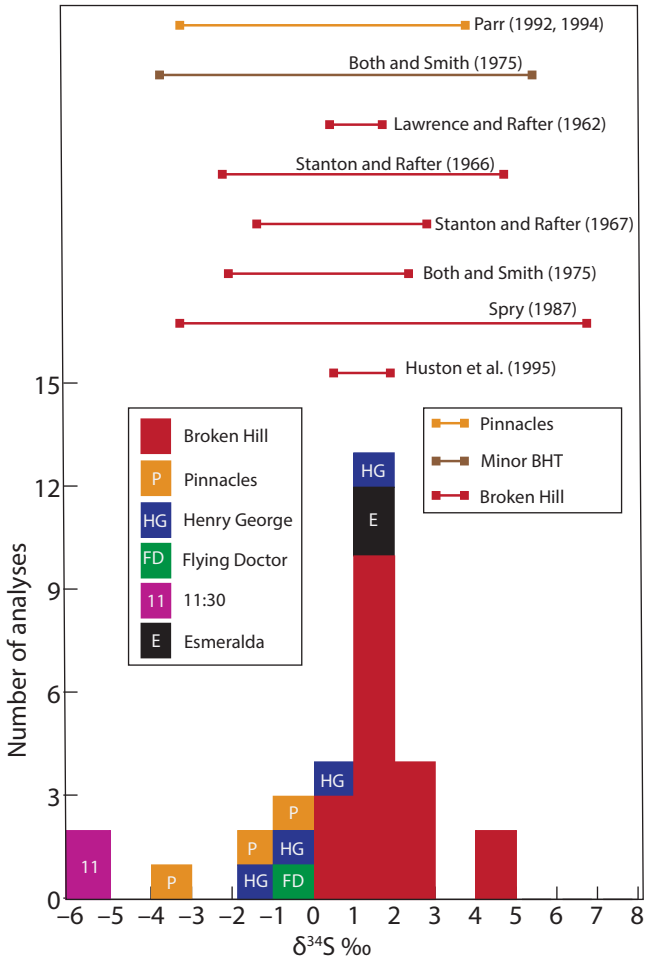

Fig. 5. (Colour online) Histogram of sulfur isotope compositions of sphalerite (this study) from the Broken Hill deposit and minor Broken Hill-type deposits (P – Pinnacles; HG – Henry George; FD – Flying Doctor; 11 – 11:30). Also shown as bar lines are the ranges of previously published sulfur isotope studies by Lawrence & Rafter (1962), Stanton & Rafter (1966, 1967), Both & Smith (1975), Spry (1987), Parr (1992, 1994*a*) and Huston *et al.* (1995). Sulfur isotope compositions of sulfides from the Pinnacles deposit, minor BHT deposits and Broken Hill from these studies are shown as orange, brown and red bar lines, respectively.

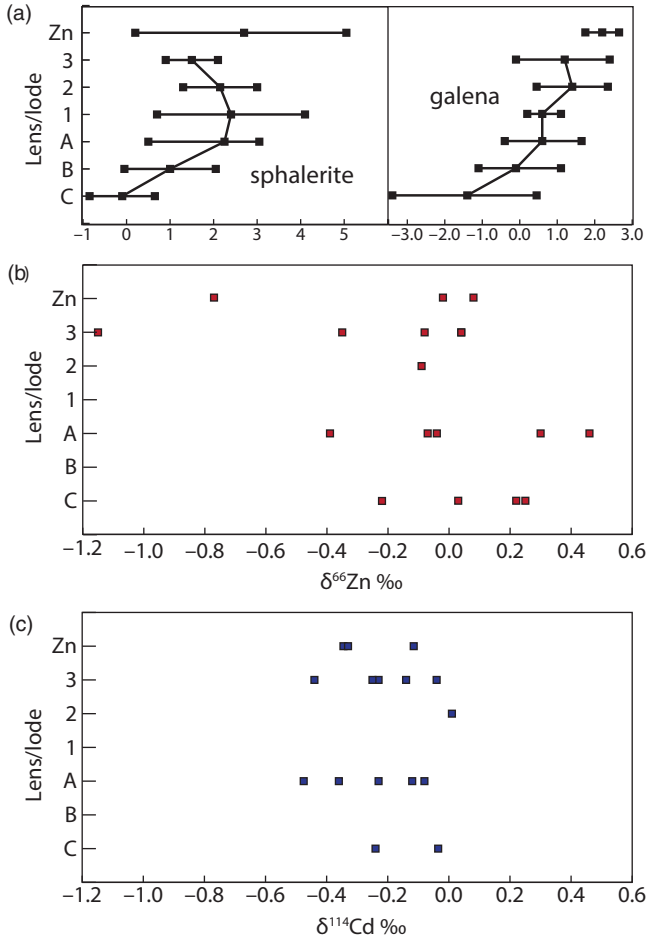

Fig. 6. (Colour online) (a) Sulfur isotope compositions of sphalerite and galena as a function of stratigraphic position (with C lode in the stratigraphic footwall) in the Broken Hill deposit. Note that isotopic compositions of sphalerite in the so-called Zinc lode from the North mine is also shown but its stratigraphic position is uncertain. Plimer (1979) proposed that it equated to either 1 lens or A lode. (b) Zinc isotope compositions as a function of stratigraphic position in the Broken Hill deposit. (c) Cadmium isotope compositions as a function of stratigraphic position in the Broken Hill deposit.

A lode; Plimer, 1979). It yields the highest average sulfur isotopic composition for sphalerite and galena for any of the orebodies.

4.b. Zinc isotopes

Values of $\delta^{66}Zn$ range from −1.15 to +0.46 ‰ ($n = 19$) for the Broken Hill deposit and from −0.97 to +0.10 ‰ ($n = 9$) for the smaller BHT deposits (Table 2). The isotopically lightest value for the smaller BHT deposits is sample JB-10-53 ($\delta^{66}Zn = -0.97$ ‰) from the Esmeralda deposit, while the isotopically heaviest sample is $\delta^{66}Zn = +0.10$ ‰ for sample JB-10-100 from the Flying Doctor deposit. Sample JB-10-53, along with samples BH-1 (3 lens), JB-10-87 (Zinc lode, North mine) and JB-10-52 (Esmeralda) have values of $\delta^{66}Zn$ of −1.15, −0.77 and −0.76 ‰, respectively, which are among the most negative values for sphalerite ever reported for an ore deposit, with that from sample BH-1 being the lowest value yet recorded. There appears to be no systematic variation of Zn isotopes from the stratigraphic footwall to the hanging wall of the Broken Hill deposit (Fig. 6b).

https://doi.org/10.1017/S0016756822000590 Published online by Cambridge University Press

4.c. Cadmium isotopes

Values of $\delta^{114}Cd$ for sphalerite from Broken Hill and smaller BHT deposits range from −0.48 to +0.01 ‰ for the Broken Hill deposit and from −1.02 to +2.59 ‰ for the smaller BHT deposits (Table 2). The isotopically lightest value is from the Henry George deposit, while the heaviest is from the 11:30 deposit. The range observed here for the BHT deposits are the most negative and positive yet reported for sphalerite from an ore deposit. Although it should be noted that Cd isotope compositions of galena from the unmetamorphosed Zhaxikang and Keyue Sedex deposits, Tibet, show the isotopically lightest ($\delta^{114}Cd = -2.19$ ‰, Zhaxikang; Wang *et al.* 2020) and the heaviest ($\delta^{114}Cd = +3.17$ ‰, Keyue; Wang *et al.* 2021) for a sulfide deposit reported to date. At first glance, the extraordinarily heavy sample from the 11:30 deposit of +2.59 ‰ may appear to be due to analytical error. However, it should be noted that the sample was analysed twice and yielded the same value (Table 2). Moreover, this same sample yielded the most isotopically light sulfur isotope value 5.11 −)‰) of any sample yet reported in the Broken Hill district. Like the Zn isotope compositions of sphalerite, there appears to be no systematic variation of Cd isotopes from the stratigraphic footwall to the hanging wall of the Broken Hill deposit for the limited number of data obtained here (Fig. 6c).

4.d. Composition of sphalerite and Zn/Cd ratios

Samples were analysed for Ag, Cd, Cu, Fe and Zn using the Agilent 5900 ICP-OES but only the Ag, Cd and Cu concentrations are accurate since the Zn and Fe are major elements (per cent levels) and thus not suitable for analysis by ICP-OES analysis, given the ppm level concentrations of Zn and Fe in the standard. The Ag, Cd and Cu concentrations of sphalerite from Broken Hill (17–2842 ppm Ag, 181–10 882 ppm Cd, 0–151 369 ppm Cu), Esmeralda (18–81 ppm Ag, 2123–2960 ppm Cd, 1664–2928 ppm Cu), Flying Doctor (196 ppm Ag, 4100 ppm Cd, 2684 ppm Cu) and Henry George (8–532 ppm Ag, 1950–2210 Cd, 576–3563 ppm Cu). To further explore the concentrations of both major- (Zn, Fe and S) and trace-element (Ag, Cd, Cu and Mn) compositions of sphalerite, a suite of ore samples containing sphalerite from the main Broken Hill deposit, as well as minor BHT deposits (Flying Doctor, Globe, Henry George) were analysed by electron microprobe (Fig. 7; Table 3). Note that samples analysed here are not the same as those analysed for Zn, Cd and S isotopes owing to the limited sample size. The Zn and Cd concentrations in sphalerite from 14 samples from the Broken Hill deposit range from 52.93 to 58.73 wt % Zn and 1740 to 2810 ppm Cd, respectively, for Zn/Cd ratios of 203 to 303 with an average of 220 (Fig. 7). The narrow range of ratios obtained by electron microprobe analysis is remarkable given the enormous size of the deposit and that the samples were collected from widely spaced localities. Samples of sphalerite were analysed from Globe ($n = 1$), Flying Doctor ($n = 2$) and Henry George ($n = 1$) and yield compositions considerably more variable than those from Broken Hill (i.e. Globe, 56.99–58.63 wt % Zn, 42–70 ppm (average Zn/Cd ratio of 1111); Flying Doctor, 51.05–56.66 wt % Zn, 2400–3420 ppm (average Zn/Cd ratios of 153 to 226); Henry George, 54.94–55.44 wt % Zn, 2410–2550 ppm Cd (average Zn/Cd ratio of 221)). The Zn/Cd ratio of 1111 for the Globe sample is anomalous relative to all other samples of sphalerite from the Broken Hill district. This is likely due to the low Fe content of the sphalerite, which is consistent with sphalerite not being buffered by a member of the system Fe–S. The Fe, Mn and Cu concentrations of sphalerite from Broken Hill range from 7.12 to 11.89 wt % Fe (average = 10.35 wt %), 0.08 to 1.02 wt % Mn (average = 0.34 wt %) and 0 to 0.09 wt % Cu (average = 0.03 wt %). Up to 0.08 wt % Ag was also obtained. The range of concentrations of Fe, Cu and Ag in sphalerite is similar to the ranges of these elements in the minor BHT deposits (6.85 to 12.93 wt % Fe, 0 to 0.04 wt % Cu, up to 0.06 wt % Ag). However, the Mn concentration is considerable lower (0.01 to 0.08 wt % Mn) in the minor BHT occurrences. The concentrations of Cd and the Zn/Cd ratios derived from electron microprobe analysis are evaluated further in this contribution rather than those obtained by ICP-OES.

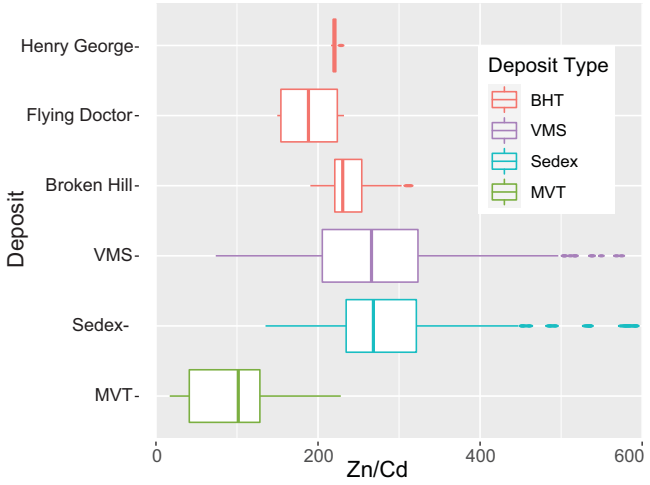

Fig. 7. (Colour online) Box and whisker plot of Zn/Cd ratios for sphalerite from the Broken Hill deposit and minor BHT deposits (Henry George and Flying Doctor). Data from the single sample from the Globe BHT deposit gave an anomalous average value of 1100 due to the low Fe content of the sphalerite, which is commensurate with sphalerite not being buffered by a member of the system Fe–S; see Table 3) Data are shown for MVT deposits: Fule, Dadongla, Jinding (Wen *et al.* 2016) and Jinding, Nanchang, Beichang (Li *et al.* 2019); VMS deposits: Cayeli (Revan *et al.* 2014), Bankshapa, Bhuyari, Biskhan, Jangaldheri (Mishra *et al.* 2021), Bukit Ketaya, Bukit Botol (Basori *et al.* 2021), Gacun (Wen *et al.* 2016); and Sedex deposits: Langshan (Wen *et al.* 2016), Mt Isa (Cave *et al.* 2020), Sullivan (Lydon & Reardon, 2000).

5. Discussion

5.a. Previous genetic models

The origin of the Broken Hill deposit and the minor BHT deposits is controversial with a variety of origins having been proposed in the vast literature on the deposit (see Greenfield, 2003). Essentially these disparate views can be distilled down to syngenetic, epigenetic and magmatic–hydrothermal models. For the syngenetic models, sulfide formed by subaqueous hydrothermal processes and subsequently underwent high-grade metamorphism, deformation and possibly partial melting (e.g. Johnson & Klingner, 1975; Laing *et al.* 1978; Mavrogenes *et al.* 2001). For the syngenetic models, there has been debate regarding whether or not the BHT deposits are Sedex deposits (e.g. Goodfellow *et al.* 1993; Sangster, 2020), a separate class of deposit (e.g. Walters, 1996; Walters *et al.* 2002; Spry & Teale, 2021) or deposits that are possibly transitional between Sedex and VMS deposits (e.g. Walters, 1998; Leach *et al.* 2005; Spry *et al.* 2010).

Epigenetic models revolve around the introduction of metals during peak metamorphism or by post-tectonic replacement (e.g. Nutman & Ehlers, 1998; Gibson & Nutman, 2004). Crawford & Maas (2009) proposed a magmatic–hydrothermal

https://doi.org/10.1017/S0016756822000590 Published online by Cambridge University Press

Table 3. Zn and Cd concentrations and Zn/Cd ratios of sphalerite from Broken Hill and BHT deposits

Deposit	Sample no.	No. analyses	Zn (wt %)	Cd (ppm)	Zn/Cd (average)
Broken Hill					
Broken Hill C lode, NBHC	JB10-140A	6	54.10–54.26	2260–2370	234
Broken Hill B lode, NBHC	JB10-125	6	53.51–54.89	1740–1860	303
Broken Hill Zinc lode, NM	JB10-82	18	53.70–54.70	2300–2610	221
Broken Hill A lode, ZC	S76-308	6	58.09–58.73	2470–2550	233
Broken Hill A lode, ZC	532-313	6	52.93–53.68	2080–2190	280
Broken Hill A Lode NBHC	532-283	6	53.70–54.33	1850–1990	280
Broken Hill SE A Lode	JB10-130A	6	53.68–54.23	1840–1950	287
Broken Hill 1 lens, NBHC	532-11 C	6	56.51–56.70	2220–2290	254
Broken Hill Lead lode, NBHC	532-35H	6	58.09–58.73	2450–2550	233
Broken Hill Lead lode, NBHC	532-34	6	54.80–55.23	2290–2430	234
Broken Hill 3 lens, NBHC	532-357	6	54.78–56.07	2640–2790	204
Broken Hill 3 lens, NBHC	532-35	6	56.40–56.89	2470–2570	225
Broken Hill 3 lens, NM	532-45	3	55.80–55.97	2420–2480	227
Broken Hill 3 lens, NM	532-73	6	53.60–54.10	2530–2810	203
Broken Hill-type					
Globe	JB10-65C	6	56.99–58.63	42–70	1111
Flying Doctor	JB10-100	6	51.05–52.19	3300–3420	153
Flying Doctor	JB10-101	6	55.39–56.66	2400–2510	226
Henry George	JB10-34	6	54.94–55.44	2410–2550	221

NBHC – New Broken Hill Consolidated mine; NM – North mine; ZC – Zinc Corporation mine.

model where they argued that the ore-forming components were derived from fractionated rift-related ferrotholeiite magmas in which fractional crystallization of Fe-rich oxide gabbros separated Cu from Pb and Zn. They suggested that magmatic fluid evolved from these magmas transported Pb and Zn in a saline-rich hydrothermal fluid and deposited metals below the seafloor.

Of these models, the epigenetic (i.e. syntectonic and post-tectonic models) of formation can be rejected since the orebodies were deformed and metamorphosed by the Olarian Orogeny. However, the syngenetic and magmatic–hydrothermal models will be considered further based on the geochemical data obtained here.

5.b. Zn/Cd ratios and Cd isotopes of sphalerite as an indicator of ore genesis

Wen *et al.* (2016) pointed out that the Cd content of sphalerite is dependent on a variety of physicochemical parameters including temperature (*T*), the nature and concentration of ligands in the ore fluid that bond to Zn and Cd, pH and the total sulfur in solution. Wen *et al.* classified Pb–Zn deposits into three groups: low-temperature (i.e. MVT deposits), high-temperature (i.e. porphyry, magmatic–hydrothermal, skarn and VMS deposits) and exhalative systems (i.e. Sedex, seafloor hydrothermal sulfides). Distinctions between the three classes of deposits were based on Cd concentrations and Zn/Cd ratios in sphalerite as well as a plot of Cd isotopes versus Zn/Cd ratios. However, an issue with Wen *et al.*'s study is that it was based on only ten occurrences, four of which were MVT deposits with single examples of a Sedex (i.e. Langshan) and a VMS deposit (i.e. Gacun).

There are several difficulties with the categorization technique proposed by Wen *et al.* (2016). Their study evaluated low- and high-temperature classes of deposits, which include different types of deposits that form under very different ore-forming conditions. For example, Wen *et al.*'s (2016) high-temperature deposits include both VMS and porphyry-style deposits, yet VMS deposits form at much lower temperatures (up to ~400 °C) than those of porphyry-style deposits that form above magmatic solidus temperatures (~600–750 °C) (Franklin *et al.* 2005; Seedorff *et al.* 2005). Volcanogenic massive sulfide deposits also generally form from low salinity fluids (i.e. equivalent to seawater compositions), although higher salinity fluids are reported in some deposits that have a magmatic component (Franklin *et al.* 2005). Metals from porphyry-style deposits are either carried in the vapour phase or from highly saline fluids (commonly >50 wt % NaCl). Finally, Wen *et al.* (2016) also provided a simplistic set of physicochemical conditions of formation for Sedex deposits proposing that they formed under reducing conditions, which is characteristic of Selwyn-type Pb–Zn Sedex deposits. Cooke *et al.* (2000) recognized the McArthur River-type Sedex deposits form from more oxidized fluids at *T* generally <200 °C, while Selwyn-type deposits form from reduced fluids at *T* >200 °C. These concerns notwithstanding, Wen *et al.* (2016) demonstrated that competing physicochemical conditions produce different Cd concentrations and Zn/Cd ratios.

https://doi.org/10.1017/S0016756822000590 Published online by Cambridge University Press

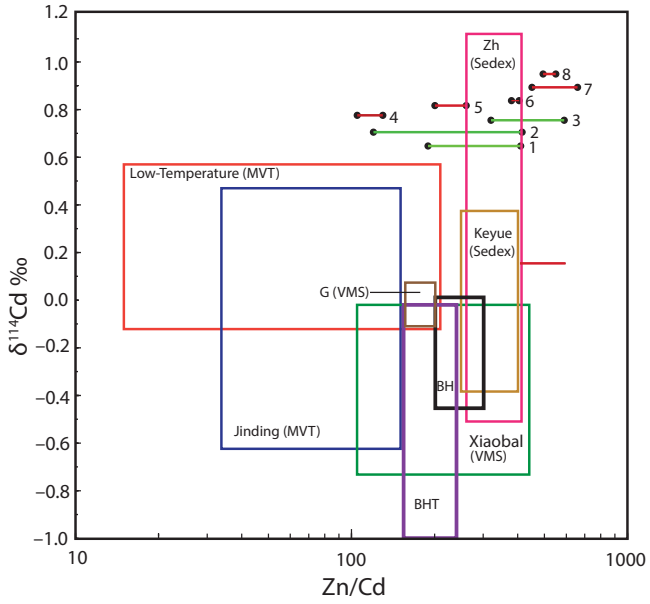

Fig. 8. (Colour online) Plot of $\delta^{114}Cd$ versus Zn/Cd ratios for sphalerite from MVT, Sedex and VMS deposits along with ranges shown for the Broken Hill and BHT deposits. Note that the boxes shown for Broken Hill and BHT deposits are based on samples of sphalerite analysed by MC-ICP-MS whereas the Zn/Cd ratios are derived from different samples (see Table 3) that were analysed by electron microprobe. Data from the literature are for the Fule, Tianbaoshan, Dadongla and Jinding MVT deposits (Wen *et al.* 2016; Zhu *et al.* 2018), Jinding MVT deposit (Li *et al.* 2019), Gacun and Xiaobaliang VMS deposits (Wen *et al.* 2016; Yang *et al.* 2022) and Keyue and Zhaxikang Sedex deposits (Wang *et al.* 2020). Abbreviations: BH – Broken Hill; BHT – Broken Hill-type; G – Gacun; Xiaobal – Xiaobaliang; Zh – Zhaxikang. Ranges of Zn/Cd ratios for sphalerite for the various deposits are shown as bar lines, which were not analysed for their Cd isotope compositions: 1 – Kanmantoo (Sedex) deposit (H. Arbon, unpub. B.Sc. Hons thesis, Univ. Adelaide, 2011); 2 – Mt Isa Cu–Pb–Zn (Sedex) deposit (Cave *et al.* 2020); 3 – Gamsberg Zn (Sedex) deposit (Höhn *et al.* 2021); 4 – Bukit Botol (VMS) deposit, massive sulfides (Basori *et al.* 2021); 5 – Bukit Botol (VMS) deposit, vein sulfides (Basori *et al.* 2021); 6 – Bankshapa VMS deposit (Mishra *et al.* 2021); 7 – Jangaldheri VMS deposit (Mishra *et al.* 2021); 8 – Biskan VMS deposit (Mishra *et al.* 2021).

Figure 8 shows a plot of the Cd isotope composition versus Zn/Cd ratios of the four MVT deposits, along with the Langshan Sedex deposit and the Gacun VMS deposit of Wen *et al.* (2016), and recent data from the Jinding MVT deposit (Li *et al.* 2019), the Keyue and Zhaxikang Sedex deposits (Wang *et al.* 2020, 2021) and the Xiaobaliang VMS deposit (Yang *et al.* 2022). Also shown are data from the Broken Hill and minor BHT deposits. Although the data of Wen *et al.* (2016) for the MVT, Sedex (Langshan) and VMS (Gacun) deposits suggest that these three deposit types can be discriminated, with MVT deposits showing the lowest Zn/Cd ratios and the Sedex deposit showing the highest Zn/Cd ratio, with the VMS deposit somewhere in between, it is clear when data for the Keyue and Zhaxikang Sedex deposits and the Xiaobaliang VMS deposits are added that these two classes of deposits overlap and cannot be distinguished. Although Cd isotope data were not obtained, Zn/Cd ratios of published sphalerite from several Sedex (Kanmantoo, Mt Isa, Gamsberg, Bleikvassli, Aclare, Sullivan) and VMS (Bankshapa, Jangaldheri, Biskan, Bhuyari, Bukit Botol, Arminius, Attu, Pontide) further show that the Zn/Cd ratios of sphalerite overlap (see Table 4) are not a useful discriminator of Wen *et al.*'s (2016) 'high-temperature' and 'exhalative' deposits.

Since the Broken Hill deposit has been regarded as a Sedex deposit by, for example, Sangster (2020), the focus here is to see if there are differences in these concentrations and ratios between sphalerite in Sedex and VMS deposits. Table 3 lists the Cd concentrations and Zn/Cd ratios of sphalerite in the Broken Hill area that were analysed by electron microprobe. The highest concentrations of Cd are generally associated with the 3 lens and Lead lode (i.e. undifferentiated 2 and 3 lenses), which is consistent with the findings of Both (1973) who determined the trace-element compositions of sphalerite concentrate in the Broken Hill orebodies. Although the Cd concentrations overlap in the current study for the various orebodies, Both (1973) found a decline in Cd content of sphalerite from 3 lens to A lode. This was not observed in the current study but is likely a result of the fewer number of samples analysed here. Given that Broken Hill and minor BHT deposits occur in metasedimentary rocks spatially associated with metaigneous rocks, it is not surprising that both sets of data for these deposits have Cd isotope compositions and Zn/Cd ratios that overlap the compositions of both Sedex and VMS deposits (Figs 7, 8). The only magmatic–hydrothermal deposit for which there are Cd isotope compositions and Zn/Cd ratio data is the Shagou deposit, China, which has Zn/Cd ratios of 154–191 and values of $\delta^{114}Cd = -0.05$ to 0 ‰. These values overlap those for MVT deposits with the Zn/Cd ratios being lower than the range observed for the Broken Hill and the minor BHT deposits. Although the number of data are limited, the range of values obtained by Wen *et al.* (2016) cannot be used to support a magmatic–hydrothermal model for the Broken Hill and minor BHT deposits.

5.c. Cd, Zn and S isotopes and the origin of Broken Hill and minor BHT deposits

By incorporating data from the present study with those of Lawrence & Rafter (1962), Stanton & Rafter (1966, 1967), Both & Smith (1975), Spry (1987), Parr (1992, 1994*a*) and Huston *et al.* (1995), sulfur isotope compositions of sulfides in the Broken Hill and minor BHT deposits show ranges of $\delta^{34}S = -3.3$ to +6.7 ‰ and −5.1 to +5.4 ‰, respectively. Plimer (1985), in recognizing that the sulfur isotope compositions were centred around 0 ‰, proposed a single primordial source of sulfur, while Parr (1992) suggested that the values near 0 ‰ were the result of sulfide formation from a modified magmatic–hydrothermal source of sulfur in which hydrothermal fluids mixed with reduced sulfur source or that magmatic sulfur was oxidized. The scenarios proposed by Plimer (1985) and Parr (1992) are supportive of a magmatic source associated with the magmatic–hydrothermal model of Crawford & Maas (2009).

Alternatively, Spry (1987) suggested an inorganic source of sulfur in which thermochemical considerations at a *T* of ~350 °C show that the range of isotopic compositions observed for Broken Hill and the minor BHT deposits occur along the pyrrhotite–magnetite join, which is the dominant assemblage in the system Fe–S–O in the Broken Hill district, although rare primary pyrite is also present (e.g. Parr, 1994*b*). A log fO_2–pH diagram incorporates the current S isotope data along with those of previously published S isotope data (Fig. 9). The temperature used here is higher than that proposed by Large *et al.* (1996) who suggested that BHT deposits were derived from slightly acid or near neutral, high salinity fluids between 100 and 250 °C. The upper temperature limit was largely based on solubility constraints of chalcopyrite. However, it should be emphasized that minor amounts of chalcopyrite are present throughout the deposit but its paucity may simply be due to the limited amount of Cu in the source rocks. Regardless, if thermochemical sulfate reduction (TSR) is assumed,

https://doi.org/10.1017/S0016756822000590 Published online by Cambridge University Press

Table 4. Cd concentrations and Zn/Cd ratios of sphalerite in MVT, VMS and Sedex deposits

Deposit	Type	No. analyses (samples)	Zn (wt %)	Cd (ppm)	Zn/Cd (average)	References
Fule	MVT	14 (8)	51.7–62.8	5238–34981	17.0–119.9 (43)	Wen *et al.* (2016)
Tianbaoshan	MVT	28 (3)	39.3–49.5	1998–4887	93.8–228.1 (140)	Wen *et al.* (2016)
Jinding	MVT	5 (4)	54.1–66.3	3184–22826	24–189 (126)	Wen *et al.* (2016)
Dadongla	MVT	5 (4)	58.7–65.1	16536–26215	24–36 (30)	Wen *et al.* (2016)
Fankou	MVT	10 (7)	55.97–62.27	1400–2700	216–389 (324)	Xuesin (1984)
Beichang	MVT	23 (23)	51.5–60.3	3160–14695	38–189 (84)	Li *et al.* (2019)
Nanchang	MVT	9 (9)	54.0–58.4	5625–22750	24–96 (46)	Li *et al.* (2019)
Maoping	MVT	23	47–61	1869–3344	156–294	Wu *et al.* (2021)
Gacun	VMS	4 (4)	51.5–63.9	2828–3476	169–213 (193)	Wen *et al.* (2016)
Bankshapa	VMS	5	60.24–62.12	1518–1569	391–407 (398)	Mishra *et al.* (2021)
Jangaldheri	VMS	9	56.30–57.62	378–1217	470–674 (558)	Mishra *et al.* (2021)
Biskhan	VMS	5	55.57–57.64	1070–1168	477–512 (498)	Mishra *et al.* (2021)
Bhuyari	VMS	6	54.53–56.07	1036–1187	463–530 (492)	Mishra *et al.* (2021)
Bukit Botol	VMS (massive)	54 (7)	65.72–66.13	5100–5700	115–130 (123)	Basori *et al.* (2021)
Bukit Botol	VMS (stringer)	24 (7)	53.48–62.35	2200–2800	216–267 (240)	Basori *et al.* (2021)
Bukit Ketaya	VMS (massive)	45 (9)	64.70–66.63	1800–2500	265–371 (320)	Basori *et al.* (2021)
Bukit Ketaya	VMS (stringer)	48 (8)	64.57–66.08	2700–5200	125–246 (218)	Basori *et al.* (2021)
Arminius	VMS	16 (8)	57.80–67.00	1000–3000*	195–670 (274)	D. J. Sandhaus (unpub. MS thesis, Virginia Polytechnic Institute and State Univ., 1981)
Cofer	VMS	35 (20)	55.80–64.70	1000–3100*	77–656 (312)	D. J. Sandhaus (unpub. MS thesis, Virginia Polytechnic Institute and State Univ., 1981)
Geco	VMS	14 (2)	58.54–58.72	2400–4700	125–244 (185)	P. G. Spry (unpub. Ph.D. thesis, Univ. Toronto, 1984)
Attu	VMS	25(10)	55.83	1900	294	Hangala (1987)
Pontide	VMS (Zone A)	16 (2)	61.80–66.40	2639–8957	78–249 (177)	Revan *et al.* (2014)
Pontide	VMS (Zone B)	1 (1)	62.7	2773	226 (226)	Revan *et al.* (2014)
Pontide	VMS (Zone C)	2 (10)	61.84–66.00	2260–3765	174–278 (219)	Revan *et al.* (2014)
Langshan	Sedex	4 (3)	1.1–34.2	34–996	316–393 (350)	Wen *et al.* (2016)
Bleikvassli	Sedex	?	58.4	1100	531	Vokes (1976)
Aclare	Sedex	1 (1)	57.4	2000	287	Spry *et al.* (1988)
Kanmantoo	Sedex	29 (4)	51.94–56.99	1200–2800	198–461 (320)	H. Arbon (unpub. B.Sc. Hons thesis, Univ. Adelaide, 2011)
Mt Isa	Sedex	357 (13)	53.08–63.86	1464–4492	135–436 (264)	Cave *et al.* (2020)
Sullivan	Sedex	222 (5)	56.20–59.72	500–3200†	180–983 (345)	Lydon & Reardon (2000)
Gamsberg	Sedex	8 (8)	51.48–52.46	900–1700	326–580 (393)	Höhn *et al.* (2021)

* below detection limits (0.11 wt % Cd) were not included.
† below detection limits (0.05 wt % Cd) were not included.

it is not possible to obtain the observed range of isotopic compositions along the pyrrhotite–magnetite join for geologically reasonable values of ionic concentrations, pH and $\delta^{34}S_{\Sigma S}$ for the ore fluid at the temperatures proposed by Large *et al.* (1996). While the range of sulfur isotope values can be explained by TSR, the range in isotope data can also be accounted for by reduced sulfur produced by TSR that is mixed with magmatic sulfur or that sulfate from seawater was reduced by biogenic processes at low temperatures (Spry, 1987). It should be noted that Both & Smith (1975) suggested that sulfur isotopic differences among BHT deposits are due to differences in the relative proportion of biogenic sulfur contributed to each deposit.

In an attempt to further evaluate ore-forming processes that may be gleaned from the sulfur isotopes obtained here, we plotted $\delta^{34}S$ versus $\delta^{114}Cd$ (Fig. 10) and $\delta^{66}Zn$ versus $\delta^{34}S$ (Fig. 11). However, these isotope pairs involving S show no systematic

https://doi.org/10.1017/S0016756822000590 Published online by Cambridge University Press

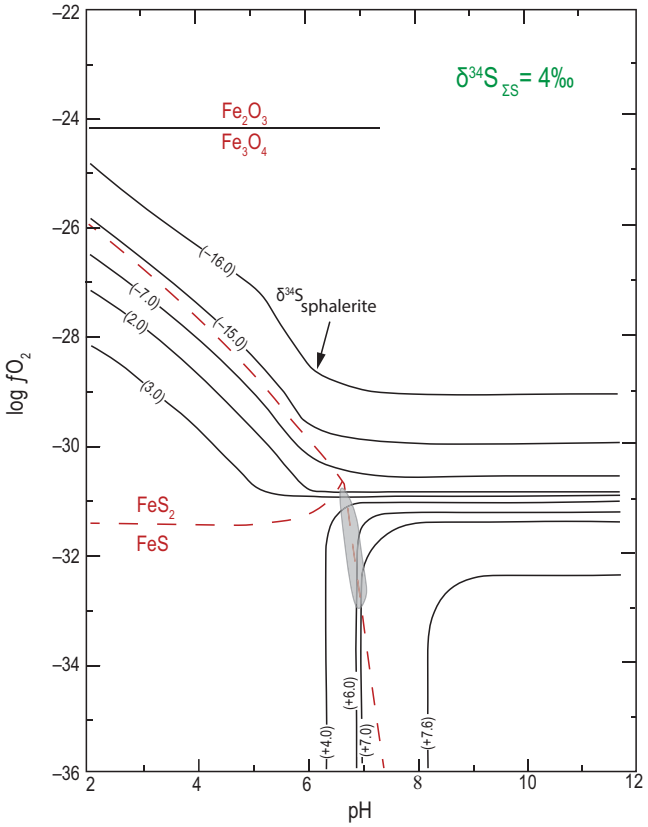

Fig. 9. (Colour online) A logfO_2–pH diagram for BHT mineralization. Sulfur isotope contours for sphalerite are drawn for $\delta^{34}S = +4$ ‰ and $T = 350$ °C. Minerals in the system Fe–S–O are shown for $\Sigma S = 0.1$ moles/kg H_2O as red dashed lines. The shaded region shows the approximate range of conditions for $\delta^{34}S$ of sphalerite over fO_2–pH range indicated (primarily along the pyrrhotite–magnetite join). Note that the shaded area starts at the pyrite–magnetite–pyrrhotite triple point to accommodate the rare presence of primary pyrite. Modified after Ohmoto (1972).

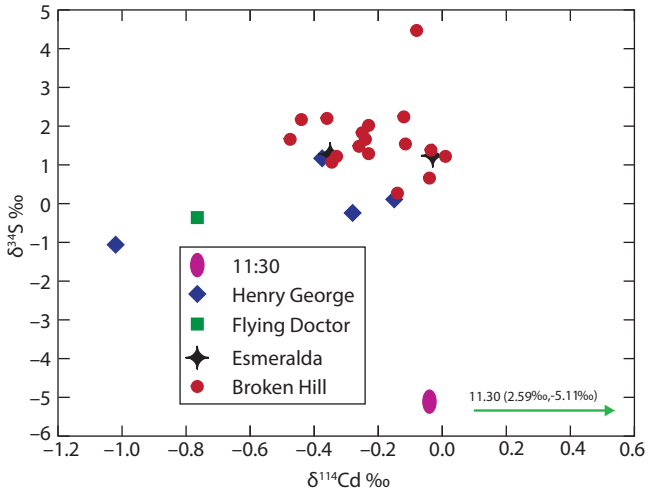

Fig. 10. (Colour online) A plot of $\delta^{34}S$ versus $\delta^{114}Cd$ for sphalerite from the Broken Hill deposit and minor BHT deposits.

variation suggesting that Zn, Cd and S were decoupled from each other. This is further demonstrated by the lack of correlation between $\delta^{66}Zn$ and $\delta^{114}Cd$ (Fig. 12). Two exceptions exist for one sample (Z3590 15.6 m) from A lode at Broken Hill and one from 11:30. The former shows the highest Zn ($\delta^{66}Zn$ = +0.46 ‰) and S ($\delta^{34}S$ = +4.47 ‰) isotope compositions in the deposit, while sample JB-10-46 from 11:30 shows the highest Cd ($\delta^{114}Cd = 2.59$ ‰) and lowest S ($\delta^{34}S$ = −5.11 ‰) isotope values for the samples analysed here.

The range of $\delta^{66}Zn$ for sphalerite from the Broken Hill deposit is among the largest (1.61 ‰) yet reported, being exceeded only by sphalerite from the Yuhuang-1 hydrothermal field (1.67 ‰; Liao *et al.* 2019). Fourteen of the 18 samples of sphalerite samples from Broken Hill have values of $\delta^{66}Zn$ that range from −0.39 to +0.46 ‰, which overlap most Zn isotope compositions reported from previous studies of MVT, Sedex and VMS deposits (Fig. 13), as well as the compositions of most igneous and sedimentary rocks (e.g. Maréchal *et al.* 2000; Toutain *et al.* 2008; Telus *et al.* 2012). A question remains as to why the remaining four Zn isotope isotopic compositions, two from Broken Hill and two from the Esmeralda deposit, yield the very negative values of $\delta^{66}Zn$ between −1.15 and −0.76 ‰.

Variations in Zn isotopes in a given hydrothermal orebody can result from a variety of processes including (Li *et al.* 2019): Rayleigh fractionation (e.g. Wilkinson *et al.* 2005; Kelley *et al.* 2009; Wang *et al.* 2020); biological processes (Li *et al.* 2019); equilibrium fractionation related to T (Mason *et al.* 2005); different Zn species in the hydrothermal fluid (Fuji *et al.* 2011); volatilization/evaporation/boiling (e.g. Paniello *et al.* 2012; Wang *et al.* 2021); and mixing of different sources of Zn (Wilkinson *et al.* 2005). Although the effects of metamorphism on the fractionation of Zn isotope compositions in natural systems have received limited attention, Xu *et al.* (2021) showed that basalts metamorphosed to the greenschist, amphibolite and eclogite facies showed no detectable fractionation. This contrasts with the observations of Pons *et al.* (2016) who showed that small isotopic variations (up to 0.16 ‰) occur in subducted Alpine serpentinites that were metamorphosed from greenschist to blueschist through to the eclogite facies. They ascribed the decrease in $\delta^{66}Zn$ to the release of oxidized Zn sulfate-rich fluids to the mantle wedge. Regardless, metamorphism to high grades would appear to only produce a very small amount (i.e. <0.2 ‰) of fractionation. Relatively small isotopic ranges were reported by S. E. Foulkes (unpub. M.Sc. thesis, Rhodes Univ., 2014) for sphalerite from the Gamsberg ($\delta^{66}Zn$ = −0.22 to −0.08 ‰, $n = 7$) and by Matt *et al.*, (2020) for sphalerite from the Balmat deposits ($\delta^{66}Zn$ = −0.30 to 0.28, $n = 47$) that were both metamorphosed to the amphibolite facies. This further supports the idea that the metamorphism does not modify the original Zn isotopes in the Broken Hill district and is not the cause for the wide isotopic range in the Broken Hill district. Owing to the intense deformation at Balmat, Matt *et al.*, (2020) showed there was a $\delta^{66}Zn$ fraction of up to 0.4 ‰ down the length of some ore bodies. They ascribed this to syntectonic isotopic fractionation that resulted from the interaction between the ore and sulfide melts that were fluxed by H_2S. Peak metamorphic conditions at Balmat reached ~640 °C and 6.5 kbar. However, given that sulfide in the Balmat deposit primarily consists of sphalerite with only minor to trace amounts of other sulfides/sulfosalts (e.g. arsenopyrite, bournonite, tetrahedrite, galena, pyrite, tennantite, chalcopyrite, jordanite, realgar; P. Matt, unpub. MS thesis, City Univ. New York, 2019) to potentially lower the melting point of a sulfide mix, there is some question regarding whether or not there was sufficient quantity of these minerals to lower the melting point to the metamorphic conditions reached at Balmat given the high melting point of sphalerite (i.e. 1827 °C). Regardless of whether or not there was a sulfide melt, or whether

https://doi.org/10.1017/S0016756822000590 Published online by Cambridge University Press

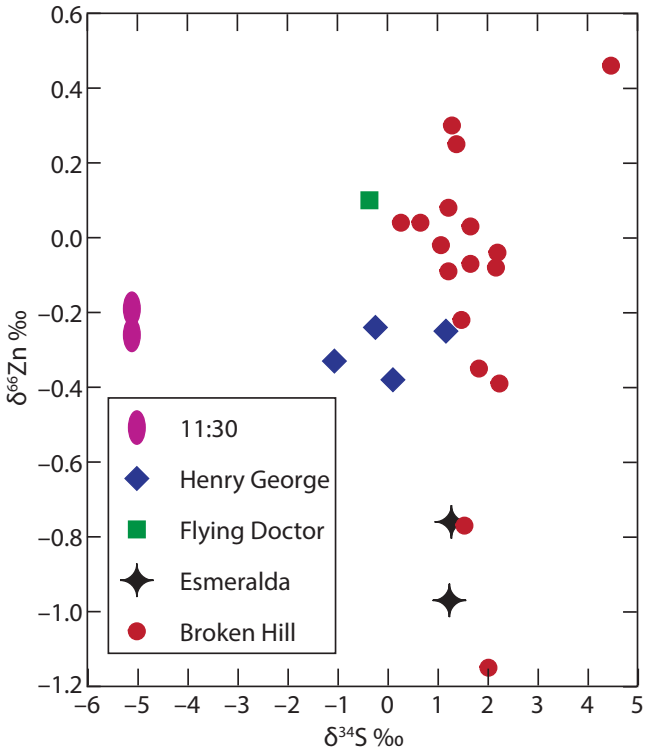

Fig. 11. (Colour online) A plot of $\delta^{66}Zn$ versus $\delta^{34}S$ for sphalerite from the Broken Hill deposit and minor BHT deposits.

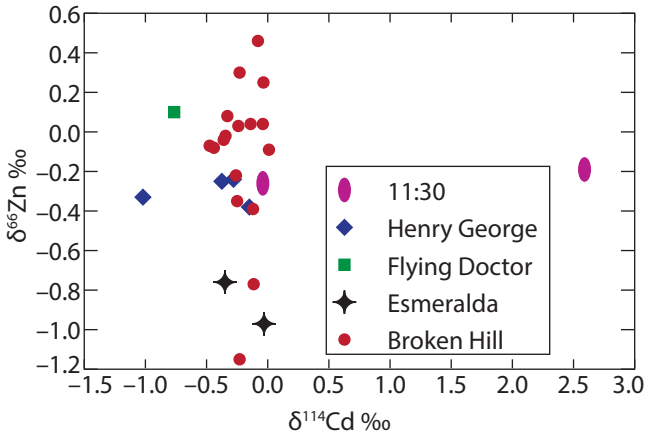

Fig. 12. (Colour online) A plot of $\delta^{66}Zn$ versus $\delta^{114}Cd$ for sphalerite from the Broken Hill deposit and minor BHT deposits.

the light Zn isotopes fractionate due to deformation in a fluid-bearing or fluid-free environment remains uncertain. However, a similar question was raised by Spry *et al.* (2008) regarding whether a partial sulfide melt was produced at Broken Hill and whether or not it was possible to produce the Pb lode ore bodies as a result of sulfide migration from the restite Zn lodes as proposed by Mavrogenes *et al.* (2001). Despite these uncertainties, fractionation of S isotopes in veins due to deformation was reported by Spry (1987) at Broken Hill and it may be the same mechanism that is responsible for some of the light Zn isotopes in the Broken Hill district where isoclinal folding exists for the first two phases of deformation that affected the Broken Hill deposit and which caused the migration of sulfides into fold hinges (e.g. Laing *et al.* 1978; Parr & Plimer, 1993).

Mechanisms involving Rayleigh fractionation may not produce the large fractionation in Zn isotopes observed in the Broken Hill and the minor BHT deposits, although it may account for the Zn isotopic compositions >0 ‰ at Broken Hill. Nonetheless, ab initio calculations by Fuji *et al.* (2011) show that negative values of $\delta^{66}Zn$ of up to 0.6 ‰ can occur in sulfides in high pH fluids (likely associated with carbonates) at low temperatures but a considerably smaller fractionation occurs under neutral to acidic fluids at higher temperatures. Regardless, Rayleigh fractionation is inconsistent with the isotopic compositions in the Esmeralda deposit and two samples from Broken Hill that have values of $\delta^{66}Zn < -0.7$ ‰ since they are hosted in clastic metasedimentary rocks rather than marbles (although carbonates are relatively common in 2 lens at Broken Hill). It is, therefore, unlikely that high pH ore fluids were associated with the formation of deposits in the Broken Hill district (including Broken Hill) and cannot account for the observed wide isotopic range.

The largest Zn isotopic variations in the solar system are associated with devolatilization processes related to the formation of terrestrial bodies where variations of several per mil have been reported (e.g. Luck *et al.* 2005; Creech & Moynier 2019). Wang *et al.* (2021), in evaluating the Zn isotopic compositions of sphalerite in the Keyue and Zhaxikang Sedex deposits, showed that vapour–liquid–solid partitioning from hydrothermal fluids would result in lighter Zn and Cd isotopes in the vapour and heavier Zn and Cd isotopes in the solid phase (i.e. sphalerite). Given the possibility that the Broken Hill and minor BHT deposits may have formed from magmatic–hydrothermal fluids (i.e. possibly in the range of 400–700 °C, see Williams-Jones & Heinrich, 2005) rather than the lower temperature fluids (i.e. <350 °C) associated with the previously discussed syngenetic model, then a vapour phase may have been generated. However, Wang *et al.* (2021) also showed that when the fraction of the initial Zn and Cd partitioned into the volatile phase is extremely high (i.e. >0.8), the resultant sphalerite precipitated from the vapour can produce very light isotopic values. This scenario could conceivably account for the very negative Zn isotopes observed in sphalerite from the Esmeralda deposit and two samples from the Broken Hill deposit even though such high partitioning of metals such as Zn and Pb into the vapour seems far-fetched. Such an extraordinarily high value is unlikely to produce the enormous amount of sphalerite in the supergiant deposit. Therefore, vaporization of the ore-forming fluid potentially associated with the magmatic–hydrothermal model does not appear to be a likely scenario to account for compositions of the Zn or Cd isotopes observed in the Broken Hill district.

Fractionation of Cd isotopes can be large with extreme values of between ~ −8 and +16 ‰ being reported for meteorites as a result of condensation and evaporation processes (e.g. Wohmbacher *et al.* 2003, 2004, 2008). Previous studies of hydrothermal ore deposits show ranges of −0.74 to +1.01 ‰ in sphalerite based on studies of the Zhaxikang VMS and Fule MVT deposits (Wen *et al.* 2016; Wang *et al.* 2020). Cadmium isotope compositions of igneous and sedimentary rocks are essentially indistinguishable with $\delta^{114}Cd$ values generally around 0 ± 0.2 ‰ (e.g. Wohmbacher *et al.* 2003; Schmitt *et al.* 2009; Liu *et al.* 2019). Values of $\delta^{114}Cd$ for sphalerite from Broken Hill and smaller BHT deposits range from −0.48 to +0.01 ‰ for the Broken Hill deposit and from $\delta^{114}Cd = -1.02$ to 2.59 ‰ for the smaller BHT deposits (Fig. 14). Although values of $\delta^{114}Cd$ for sphalerite from Broken Hill overlap those of igneous and sedimentary rocks, 10 of the 17 samples analysed range from $\delta^{114}Cd = -0.48$ to −0.23 ‰ suggesting that some mechanism other than hydrothermal processes,

https://doi.org/10.1017/S0016756822000590 Published online by Cambridge University Press

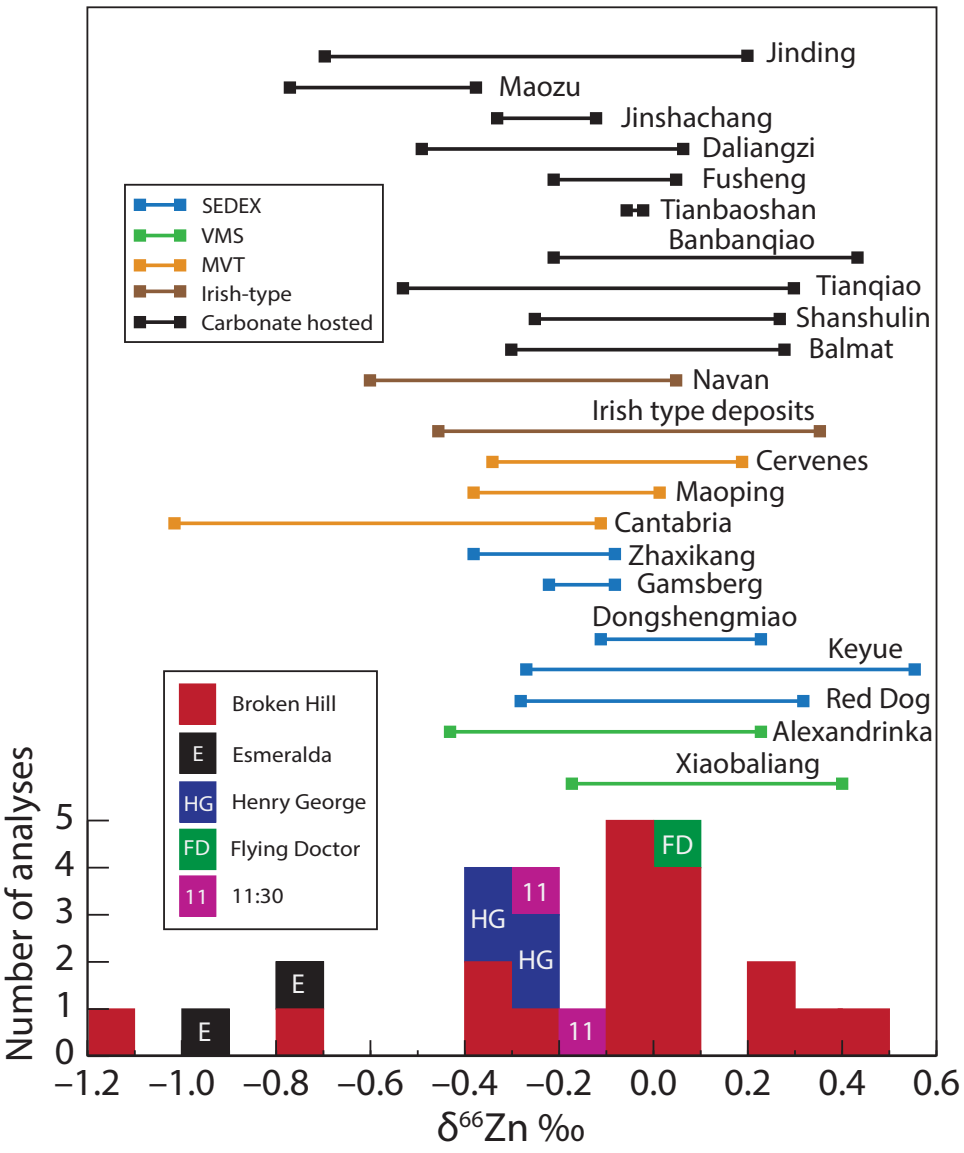

Fig. 13. (Colour online) Histogram of $\delta^{66}Zn_{AA\text{-}ETH}$, compositions of sphalerite from the Broken Hill deposit and minor Broken Hill-type deposits. Also shown as bar lines are the ranges of $\delta^{66}Zn$ for sphalerite from the Dongshengmiao (Gao *et al.* 2018), Gamsberg (S. E. Foulkes, unpub. M.Sc. thesis, Rhodes Univ., 2014), Keyue (Wang *et al.* 2021), Red Dog (Kelley *et al.* 2009) and Zhaxikang (Wang *et al.* 2018, 2021) Sedex deposits; the Alexandrinka (Gao *et al* 2018) and Xiaobaliang (Yang *et al.* 2022) VMS deposits; the Cantabria (Pašava *et al.* 2014), Cévennes (Albarède, 2004), Jinding (Deng *et al.* 2017; Li *et al.* 2019), Maoping (Wu *et al.* 2021) and Wuishe (Zhu *et al.* 2018) MVT deposits; Irish-type deposits including Navan (Wilkinson *et al.* 2005; Gangevin *et al.* 2012) and the Balmat (Matt *et al.*, 2020), Banbanqiao, Tianqiao (Zhou *et al.* 2014*b*), Daliangzi, Fusheng, Jinshachang, Mazou, Tianbaoshan (Xu *et al.* 2020) and Shanshulin (Zhou *et al.* 2014*a*) carbonate-hosted Pb–Zn or Zn deposits. Note that the anomalous value of sample of $\delta^{66}Zn = +1.05$ ‰ for late-stage sphalerite that was obtained by Wilkinson *et al.* (2005) from the Galmoy Irish-type Zn–Pb deposit is not shown on this figure. The reader can view the individual data points for most of the deposits shown here in Wang *et al.* (2018, 2021).

where Cd was extracted from the meta-igneous and metasedimentary package associated with the Zn–Pb deposits in the Broken Hill district, was responsible. In a Cd, S and Zn isotope study of the Xiaobaliang VMS deposit, Yang *et al.* (2022) proposed that the values of $\delta^{114}Cd_{NIST\text{-}3108}$ values for sphalerite, which range from −0.74 to −0.08 ‰, are the result of biological processes that enrich the fluid in the light Cd isotope, resulting in the precipitation of sulfides with light values of $\delta^{114}Cd$. Such processes are considered here.

5.d. A biological syndepositional model for the formation of the Broken Hill deposit and minor BHT deposits

Although the S isotopic compositions of sphalerite can be interpreted in the light of a magmatic–hydrothermal or a syngenetic model, where TSR occurs at a temperature of around 350 °C, neither model can account for the wide range of Zn and Cd isotope compositions of sphalerite. Microbially mediated dissimilatory sulfate reduction to H_2S produces isotopically light H_2S with $\Delta^{34}S_{SO4\text{-}H2S}$ up to 72 ‰ (e.g. Canfield & Teske, 1996; Balci *et al.* 2007). However, biological processes are also likely to be important for Zn and Cd (e.g. Li *et al.* 2019). Although fractionation factors associated with biological processes are not large (1.0002 to 1.0008; Abouchami *et al.* 2013), biological partial assimilation of Cd from seawater can generate a range of $\delta^{114}Cd$ of 7 ‰ in surface waters as a result of the uptake of dissolved Cd by photosynthesis (e.g. Lacan *et al.* 2006; Ripperger *et al.* 2007; Schmitt *et al.* 2009; Wen *et al.* 2016), while a range of $\delta^{66}Zn$ of up to ~0.7 ‰ occurs as a result of biological processes (e.g. Conway & John, 2014; John & Conway 2014; Zhao *et al.* 2014) (Fig. 15). Theoretical calculations and experimental studies of Fuji *et al.* (2011) and Marković *et al.* (2017), respectively, show that organic compounds (e.g. Zn-carboxylate) generally have heavier isotopic compositions than Zn^{2+}, which can result in sphalerite having very low $\delta^{66}Zn$ values in a low *T* solution (i.e. <100 °C). Li *et al.* (2019) suggested that Cd, like Zn, may have bonded to carboxylate molecules in hydrothermal solutions resulting in light isotopic values for sphalerite.

However, two features of the Zn and Cd isotope ranges for sphalerite from Broken Hill need to be addressed: why there is no apparent linear relationship between Zn and Cd isotopic

https://doi.org/10.1017/S0016756822000590 Published online by Cambridge University Press

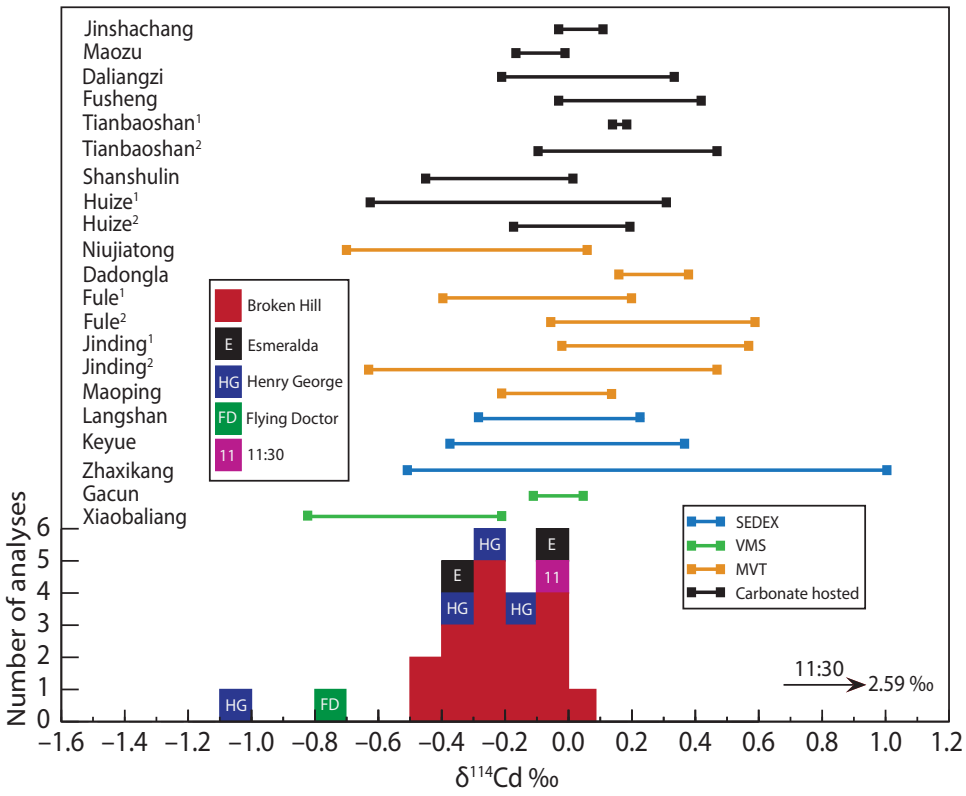

Fig. 14. (Colour online) Histogram of $\delta^{114}Cd_{NIST\ SRM\ 3108}$ compositions of sphalerite from the Broken Hill deposit and minor Broken Hill-type deposits. Also shown as bar lines are the ranges of $\delta^{114}Cd$ for sphalerite from the Keyue (Wang *et al.* 2021), Langshan (Wen *et al.* 2016) and Zhaxikang (Wang *et al.* 2020, 2021) Sedex deposits; Gacun (Wen *et al.* 2016) and Xiaobaliang (Yang *et al.* 2022) VMS deposits; Dadongla (Wen *et al.* 2016), Fule[1,2] (Zhu *et al.* 2013[1]; Wen *et al.* 2016[2]), Jinding[1,2] (Wen *et al.* 2016[1]; Li *et al.* 2019[2]), Maoping (Wu *et al.* 2021) and Niujiatong (Zhu *et al.* 2013) MVT deposits; and Daliangzi, Fusheng, Jinshachang, Mazou, Tianbaoshan[1] (Xu *et al.* 2020), Tianbaoshan[2] (Zhu *et al.* 2016) Huize[1,2] (Zhu *et al.* 2013[2], 2021[1]) and Shanshulin carbonate-hosted Pb–Zn or Zn deposits (Zhu *et al.* 2013). The reader can view the individual data points for some of the deposits shown here in Li *et al.* (2019), although their data are reported as $\delta^{114}Cd_{SPEX}$.

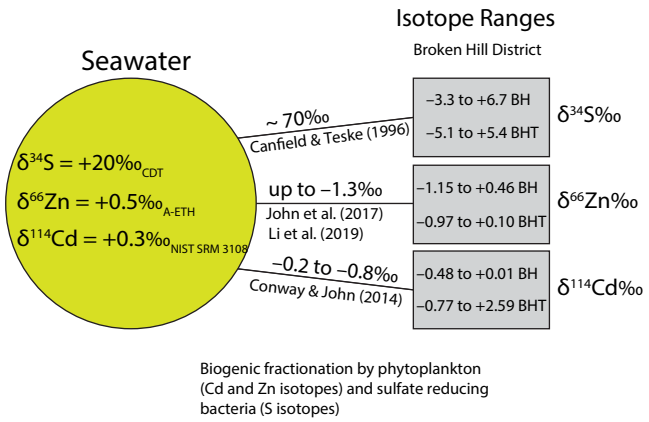

Fig. 15. (Colour online) Schematic plot showing the fractionation of Zn, Cd and S isotopes as a result of biogenic sulfate reduction (BSR) and its relationship to isotopic values reported for these elements for sulfides from the Broken Hill deposit and minor BHT deposits. For the sulfur isotope fractionation, we include the amount of fractionation caused by bacterial sulfate reduction for $\delta^{34}S$ of up to ~70 ‰ reported by Canfield & Teske (1996) and Lefticariu *et al.* (2017) and a sulfur isotope value of +20 ‰ of Strauss (2004) for Proterozoic seawater. A value of $\delta^{66}Zn = +0.5$ ‰ for deep seawater (John & Conway 2014; Zhao *et al.* 2014) with preferential uptake of light isotopes during biological assimilation by as much as −1.3 ‰ (i.e. the sum of values for biological assimilation (up to 0.7 ‰) and scavenging/adsorption (−0.3 to −0.6 ‰) (Conway & John 2014; John & Conway 2014; Li *et al.* 2019) and scavenging/adsorption of Zn on phytoplankton membranes causing an additional isotopic fraction of $\delta^{66}Zn$ of −0.3 to −0.6 ‰. A value of $\delta^{114}Cd$ of +0.3 ‰ is given for deep seawater (e.g. Chen *et al.* 2021). Biological fractionation causes phytoplankton to have values of $\delta^{114}Cd$ lower by 0.2 to 0.8 ‰.

compositions (see Fig. 12) and why the range of isotopic values for Cd is smaller than that for Zn isotopes. Cadmium and Zn behave differently with regards to biological productivity. While Zn can be adsorbed and assimilated by phytoplankton, the scavenging of isotopically heavy Zn onto biological particles, which sink through the water column, leave the remaining fluid characterized by lighter Zn isotope compositions (John *et al.* 2017). Scavenging/adsorption can lower the Zn isotope compositions by −0.3 to −0.6 ‰ (Li *et al.* 2019). Therefore, the sum of values related to preferential uptake of light isotopes during biological processes is as much as −1.3 ‰ (i.e. the sum of values for biological assimilation (up to 0.7 ‰; Conway & John, 2014; John & Conway, 2014) and scavenging/adsorption (−0.3 to −0.6 ‰; Li *et al.* 2019)). On the other hand, Cd is not scavenged by biological particles but is controlled by biological assimilation as it substitutes for P. If Zn in the Broken Hill area was released from organic material during decay to form sphalerite this process could result in the light isotopic composition of both Zn and Cd. Alternately, sphalerite formation from the residual seawater would not account for the Cd isotope composition because surface seawater trends to high values of $\delta^{114}Cd$.

A similar explanation for the small range in Cd isotopes compared to Zn isotopes, a feature observed in sphalerite from the Broken Hill area, was proposed by John *et al.* (2017) for the Neoproterozoic dolostones from the Nuccaleena Formation, South Australia. In the Nuccaleena dolostone, Cd was buried in biological material (i.e. phytoplankton) to produce light Cd isotope compositions, while scavenging of heavy Zn left surface seawater with light Zn isotope compositions. Organic matter formed in surface seawater when buried will produce a larger isotopic range for Zn than Cd.

A mechanism involving Zn and Cd being bonded to organic molecules best accounts for the light Zn and Cd isotopic compositions in the Broken Hill district, including the light isotopic values from the Flying Doctor ($\delta^{114}Cd = -0.77$ ‰) and Henry George ($\delta^{114}Cd = -1.02$ ‰). This scenario is analogous to biogenic processes proposed by Li *et al.* (2019) to explain similar Zn, Cd and S

https://doi.org/10.1017/S0016756822000590 Published online by Cambridge University Press

isotope compositions for sulfides from the giant Jinding MVT deposit, China, and by Yang *et al.* (2022) to account for the isotopically light Cd and S isotope values of sphalerite in the Xiaobaliang Cu–Au VMS deposit, China. Fractionation by biogenic sulfate reduction (BSR) is consistent with the process proposed by Both & Smith (1975) to explain the differences in S isotopes in the district. To this end, Heimann *et al.* (2013) also reported C and O isotopes values in calcite from the Esmeralda and Broken Hill deposits (the two deposits that show the most negative values of $\delta^{66}Zn$; Table 2), which range from −25 to −21 ‰ for $\delta^{13}C_{VPDB}$ and +10 to +11.0 ‰ for $\delta^{18}O_{SMOW}$, respectively. The low carbon isotope values also overlap ($\delta^{13}C_{VPDB} = -26$ to −14 ‰) for graphite in graphitic schists in the southern Curnamona province (including the Broken Hill deposit) and calcite at the RW Iron Clad and Little Broken Hill BHT prospects (M. Schuler *et al.*, The Broken Hill Line of Lode Study, unpub. report to Pasminco Mining Company, 1993; Bierlein *et al.* 1996). Biogenic processes occur at low temperatures (i.e. <100 °C). Notwithstanding the proposal here that biological processes are important in producing the Zn, Cd and S isotopic compositions reported for sphalerite in the Broken Hill district, the cause of the outlier value of $\delta^{114}Cd = +2.59$ ‰, coupled with the isotopically lightest value of $\delta^{34}S$ of −5.11 ‰, for the samples studied here from the small 11:30 deposit remains unknown. However, these anomalous isotopic values may be due to kinetic and/or equilibrium effects similar to those responsible for the isotopically anomalous value of $\delta^{66}Zn > +1$ ‰ reported by John *et al.* (2008) for sulfides in active hydrothermal vents on the seafloor.

6. Conclusions

Geological and geochemical considerations suggest that the Broken Hill deposit as well as minor BHT deposits likely formed by either syngenetic processes at T <350 °C or from magmatic–hydrothermal fluids at a T of between 400 and 700 °C. Although S isotope studies are compatible with either process, Cd and Zn isotope studies are incompatible with high T processes because both the lighter isotopes for both isotopic systems will fractionate into the vapour phase leaving sphalerite exhibiting heavy isotopic compositions. Even though the S, Cd and Zn isotope values show no correlation with each other, suggesting they were decoupled, the isotopic ranges are commensurate with fractionation being caused by low-temperature biogenic processes.

The Zn and Cd isotope variations for sphalerite from the Broken Hill deposit and minor BHT deposits are among the largest yet reported. Although biogenic processes appear to be the most likely explanation for the isotopically light values reported for both isotopes, fractionation caused by mechanical processes whereby the lighter isotope Zn and Cd isotopes migrate more easily in a fluid assisted or depleted system is uncertain, but this remains a possibility given the extreme deformation that resulted in two isoclinal fold episodes at Broken Hill and the migration of sulfides into fold hinges.

Syngenetic scenarios for the Broken Hill deposit have previously considered it being a VMS or Sedex deposit. Although Cd isotopes have been combined with the Zn/Cd isotope ratio of sphalerite to classify Pb–Zn deposits in the past and may have helped in distinguishing these two deposit models, such an exercise is fraught with problems. Although MVT deposits tend to have lower Zn/Cd ratios in sphalerite than those formed by high-temperature (e.g. VMS) and exhalative (Sedex) systems, the Zn/Cd ratios for VMS and Sedex deposits overlap and cannot be used to distinguish between these deposit types. Sphalerite from the Broken Hill and BHT deposits have average Zn/Cd ratios for sphalerite that range from 203 to 303 and fit within the overlap region for Sedex and VMS deposits. This is hardly surprising given the spatial association of sulfide mineralization with bimodal mafic and felsic igneous rocks within a thick package of metasedimentary rocks.

Acknowledgements. Funding for the electron microprobe facility used in this research was provided by the National Science Foundation under award number EAR-1625422. Dan-Layton Matthews and Evelyne Leduc Queen's Facility for Isotope Research (Queen's University, Canada) are kindly thanked for providing sulfur isotope standards, while Ben Johnson (ISU) helped with S isotope analyses. Assistance with drafting by Justin Glenn is gratefully appreciated. The reviews of Peter Matt and Da Wang are greatly appreciated and improved the quality of the manuscript.

References

Abouchami W, Galer SJG, Horner TJ, Rehkämper M, Wombacher F, Xue Z, Lambelet M, Gault-Ringold M, Stirling CH, Schönbächler M, Shiel AE, Weis D and Holdship PF (2013) A common reference material for cadmium isotope studies – NIST SRM 3108. *Geostandards and Geoanalytical Research* **37**, 5–17.

Albarède F (2004) The stable isotope geochemistry of copper and zinc. *Reviews in Mineralogy and Geochemistry* **55**, 409–27.

Andrews EC (1922) *The Geology of the Broken Hill District*. Geological Survey of New South Wales Memoir 8. Sydney: William Applegate Gullick, Government Printer, 432 pp.

Archer C, Andersen MB, Cloquet C, Conway TM, Dong S, Ellwood M, Moore R, Nelson J, Rehkämper M, Rouxel O, Samanta M, Shin K-C, Sohrin Y, Takan S and Wasylenki L (2017) Inter-calibration of a proposed new primary reference standard AA-ETH Zn for zinc isotopic analysis. *Journal of Analytical Atomic Spectrometry* **32**, 415–19.

Archer C and Vance D (2004) Mass discrimination correction in multiple-collector plasma source mass spectrometry: an example using Cu and Zn isotopes. *Journal of Analytical Atomic Spectrometry* **19**, 656–65.

Balci N, Shanks WC III, Mayer B and Mandernack KW (2007) Oxygen and sulfur isotope systematics of sulfate produced by bacterial and abiotic oxidation of pyrite. *Geochimica et Cosmochimica Acta* **71**, 3796–811.

Barnes RG, Stevens BPJ, Stroud WJ, Brown RE, Willis IL and Bradley GM (1983) Zinc, manganese and iron-rich rocks and various minor rock types. *Records of the Geological Survey of New South Wales* **21**, 289–323.

Basori MBI, Gilbert SE, Zaw K and Large RR (2021) Geochemistry of sphalerite from the Permian volcanic-hosted massive sulphide (VHMS) deposits in the Tasik Chini area, Peninsular Malaysia: constraints for ore genesis. *Minerals* **11**, 728. doi: 10.3390/min11070728.

Baumgartner RJ, Kunzmann M, Spinks S, Bian X, John SG, Blaikie TN and Hu S (2021) Zinc isotope composition of the Proterozoic clastic-dominated McArthur River Zn-Pb-Ag deposit, northern Australia. *Ore Geology Reviews* **39**, 104545. doi: 10.1016/j.oregeorev.2021.104545.

Bierlein FP, Ashley PM and Seccombe, PK (1996) Origin of hydrothermal Cu–Zn–Pb mineralisation in the Olary Block, South Australia: evidence from fluid inclusions and sulphur isotopes. *Precambrian Research* **79**, 281–305.

Birch WD (1999) The minerals. In *Minerals of Broken Hill* (ed. WD Birch), pp. 88–256. Broken Hill: Broken Hill City Council.

Both RA (1973) Minor element geochemistry of sulphide minerals in the Broken Hill lode (N. S.W.) in relation to the origin of the ore. *Mineralium Deposita* **8**, 349–69.

Both RA and Smith JW (1975) A sulfur isotope study of base-metal mineralization in the Willyama Complex, western New South Wales. *Economic Geology* **70**, 308–18.

Both RA and Stumpfl EF (1987) Distribution of silver in the Broken Hill orebody. *Economic Geology* **82**, 1037–43.

Burton GR (1994) *Metallogenic Studies of the Broken Hill and Euriowie Blocks, New South Wales. 3, Mineral Deposits of the South-Eastern Broken Hill Block.*

https://doi.org/10.1017/S0016756822000590 Published online by Cambridge University Press

Bulletin of the Geological Survey of New South Wales 32. Sydney: Geological Survey of New South Wales, 100 pp.

Canfield DE and Teske A (1996) Late Proterozoic rise in atmospheric oxygen concentration inferred from phylogenetic and sulphur-isotope studies. *Nature* **382**, 127–32.

Cave B, Lilly R and Barovich K (2020) Textural and geochemical analysis of chalcopyrite, galena and sphalerite across the Mount Isa Cu to Pb-Zn transition: implications for a zoned Cu-Pb-Zn system. *Ore Geology Reviews* **124**, 103647. doi: 10.1016/j.oregeorev.2020.103647.

Chantler CT, Olsen K, Dragoset RA, Chang J, Kishore AR, Kotochigova SA and Zucker DS (2005) *X-ray Form Factor, Attenuation and Scattering Tables (Version 2.1)*. Gaithersburg, MD: National Institute of Standards and Technology.

Chapman JB, Mason TFD, Weiss DJ, Coles BJ and Wilkinson JJ (2004) An adapted column chemistry procedure for separation of Fe, Cu and Zn from geological matrices, and natural Zn isotopic variations in geological standard reference materials BCR-027, BCR-030 and NOD-P-1. *Geological Society of America Abstracts with Programs* **36**, 448.

Chapman, JB, Mason TFD, Weiss DJ, Coles BJ and Wilkinson JJ (2006) Chemical separation and isotopic variations of Cu and Zn from five geological reference materials. *Geostandards and Geoanalytical Research* **30**, 5–16.

Chen L, Little SH, Kreissig KI, Severmann S and McManus J (2021) Isotopically light Cd in sediments underlying oxygen deficient zones. *Frontiers in Earth Science* **9**, 623720. doi: 10.3389/feart.2021.623720.

Cloquet C, Rouxel O, Carignan J and Libourel G (2005) Natural cadmium isotopic variations in eight geological reference materials (NIST SRM 2711, BCR 176, GSS-1, GXR-1, GXR-2, GSD-12, Nod-P-1, Nod-A-1) and anthropogenic samples, measured by MC-ICP-MS. *Geostandards and Geoanalytical Research* **29**, 95–106.

Conor CHH and Preiss WV (2008) Understanding the 1720–1640 Ma Palaeoproterozoic Willyama Supergroup, Curnamona Province, southeastern Australia: implications for tectonics, basin evolution and ore genesis. *Precambrian Research* **166**, 297–317.

Conway T and John S (2014) The biogeochemical cycling of zinc and zinc isotopes in the North Atlantic Ocean. *Global Biogeochemical Cycles* **28**, 1111–28.

Cooke DR, Bull SW, Large RR and McGoldrick PJ (2000) The importance of oxidized brines for the formation of Australian Proterozoic stratiform sediment-hosted Pb-Zn (Sedex) deposits. *Economic Geology* **95**, 1–17.

Crawford AJ and Maas R (2009) A magmatic-hydrothermal origin for the giant Broken Hill deposit. *Geoscience Australia Record* **2009/28**, 28–30.

Creech JB and Moynier F (2019) Tin and zinc stable isotope characterisation of chondrites and implications for early Solar System evolution. *Chemical Geology* **511**, 81–90.

Deng J, Wang C, Bagas L, Selvaraja V, Jeon H, Wu B and Yang L (2017) Insights into ore genesis of the Jinding Zn-Pb deposit, Yunnan Province, China: evidence from Zn and in-situ S isotopes. *Ore Geology Reviews* **90**, 943–57.

Dong Y-B, Barnes RG, Both RA and Sun SS (1987) Regional stable isotope and fluid inclusion study of vein-type mineralization in the Broken Hill Block, New South Wales, Australia. *Transactions of the Institute of Mining and Metallurgy* **9**, B15–B30.

Donovan JJ, Singer JW and Armstrong JT (2016) A new EPMA method for fast trace element analysis in simple matrices. *American Mineralogist* **101**, 1839–53.

Donovan JJ and Tingle TN (1996) An improved mean atomic number correction for quantitative microanalysis. *Journal of Microscopy* **2**, 1–7.

Findlay D (1994) Boudinage, a reinterpretation of the structural control on the mineralization at Broken Hill. *Australian Journal of Earth Science* **41**, 387–90.

Franklin JM, Gibson HL, Jonasson IR and Galley AG (2005) Volcanogenic massive sulfide deposits. In *Economic Geology: One Hundredth Anniversary Volume* (eds JW Hedenquist, JFH Thompson, RJ Goldfarb and JP Richards), pp. 523–60. Littleton, Colorado: Society of Economic Geologists.

Frost BR, Swapp S and Mavrogenes J (2011) Textural evidence for extensive melting of the Broken Hill orebody. *Economic Geology* **101**, 1117–37.

Fuji T, Moynier F, Pons, M-L and Albarède F (2011) The origin of Zn isotope fractionation in sulfides. *Geochimica et Cosmochimica Acta* **75**, 7632–43.

Gagnevin D, Boyce AJ, Barrie CD, Menuge JF and Blakeman RJ (2012) Zn, Fe and S isotope fractionation in a large hydrothermal system. *Geochimica et Cosmochimica Acta* **88**, 183–98.

Gagnevin D, Menuge JF, Kronz A, Barrie C and Boyce AJ (2014) Minor elements in layered sphalerite as a record of fluid origin, mixing, and crystallization in the Navan Zn-Pb ore deposit, Ireland. *Economic Geology* **109**, 1513–28.

Gao Z, Zhu X, Sun J, Luo Z, Bao C, Tang C and Ma J (2018) Spatial evolution of Zn-Fe-Pb isotopes of sphalerite within a single ore body: a case study from the Dongshengmiao ore deposit, Inner Mongolia, China. *Mineralium Deposita* **53**, 55–65.

Gibson GM and Nutman AP (2004) Detachment faulting and bimodal magmatism in the Palaeoproterozoic Willyama Supergroup, south-central Australia: keys to recognition of a multiply deformed Precambrian metamorphic core complex. *Journal of the Geological Society, London* **161**, 55–66.

Goodfellow WD, Lydon JW and Turner RJW (1993) Geology and genesis of stratiform sediment hosted (SEDEX) zinc-lead-silver sulphide deposits: mineral deposit modeling. In *Mineral Deposit Modeling* (eds RV Kirkham, WD Sinclair, RI Thorpe and JM Duke), pp. 201–51. Geological Association of Canada Special Paper 40.

Grassineau NV (2006) High-precision EA-IRMS analysis of S and C isotopes in geological materials. *Applied Geochemistry* **21**, 756–65.

Greenfield J (2003) A critical review of Broken Hill ore system models. Commonwealth Scientific Industrial Research Organisation and Exploration Report 1160R, 192 pp.

Groves IM, Groves DI, Bierlein FP, Broome J and Penhall J (2008) Recognition of the hydrothermal feeder to the structurally inverted, giant Broken Hill deposit, New South Wales, Australia. *Economic Geology* **103**, 1389–94.

Hangala LS (1987) *The Early Proterozoic Zn-Pb-Cu Massive Sulfide Deposit at Attu, SW Finland*. Bulletin of the Geological Survey of Finland 341. Espoo: Geologian Tutkimuskeskus, 69 pp.

Heimann A, Spry PG, Teale GS, Leyh WR, Conor CHH, Mora G and O'Brien JJ (2013) Geochemistry and genesis of low-grade metasediment-hosted Zn-Pb-Ag mineralization, southern Proterozoic Curnamona province, Australia. *Journal of Geochemical Exploration* **128**, 97–116.

Hodgson CJ (1975) The geology and geological development of the Broken Hill lode, in the New Broken Hill Consolidated mine Australia part II: mineralogy. *Journal of the Geological Society Australia* **22**, 33–50.

Hohl SV, Galer SJG, Gamper A and Becker B (2017) Cadmium isotopic variations in Neoproterozoic carbonates – a tracer of biogenic production? *Geochemical Perspectives Letter* **312**, 243–53.

Höhn S, Frimmel HE and Westley P (2021) Syn-metamorphic sulfidation of the Gamsberg zinc deposit, South Africa. *Mineralogy and Petrology* **115**, 709–28.

Huston DL, Power M, Gemmell JB and Large RR (1995) Design, calibration and geological application of the first operational Australian laser ablation sulphur isotope microprobe. *Australian Journal of Earth Sciences* **42**, 549–55.

Huston DL, Stevens B, Southgate PN, Muhling P and Wyborn L (2006) Australian Zn-Pb-Ag ore-forming systems: a review and analysis. *Economic Geology* **101**, 1117–37.

John SG and Conway TM (2014) A role for scavenging in the marine biogeochemical cycling of zinc and zinc isotopes. *Earth and Planetary Science Letters* **394**, 159–67.

John SG, Kunzmann M, Townsend EJ and Rosenberg AD (2017) Zinc and cadmium stable isotopes in the geological record: a case study from the post-snowball Earth Nuccaleena cap dolostone. *Palaeogeography, Palaeoclimatology, Palaeoecology* **466**, 202–8.

John SG, Rouxel OJ, Craddock PR, Engwall AM and Boyle EA (2008) Zinc stable isotopes in seafloor hydrothermal vent fluids and chimneys. *Earth and Planetary Science Letters* **269**, 17–28.

Johnson IR and Klingner GD (1975) The Broken Hill ore deposit and its environment. In *Economic Geology of Australia and Papua New Guinea, 1* (ed. CL Knight) pp. 476–91. Parkville, Victoria: Australasian Institute of Mining and Metallurgy.

Katz MB (1976) Lineament tectonics of the Willyama and its relationship to the Adelaide aulocogene. *Journal of the Geological Society of Australia* **23**, 275–85.

Kelley KD, Wilkinson JJ, Chapman JB, Crowther HL and Weiss DJ (2009) Zinc isotopes in sphalerite from base metal deposits in the Red Dog district, northern Alaska. *Economic Geology* **104**, 767–73.

Lacan F, Francois R, Ji Y and Sherrell RM (2006) Cadmium isotopic composition in the ocean. *Geochimica et Cosmochimica Acta* **70**, 5104–18.

Laing WP, Marjoribanks RW and Rutland RWR (1978) Structure of the Broken Hill mine area and its significance for the genesis of the ore bodies. *Economic Geology* **73**, 1112–36.

Large R, Bodon S, Davidson G and Cooke D (1996) The chemistry of BHT ore formation – one of the keys to understanding the differences between SEDEX and BHT deposits. In *New Developments in Broken Hill-Type Deposits* (eds J Pongratz and GJ Davidson), pp. 105–11. CODES Special Publication 1. Hobart: Centre for Ore Deposit and Exploration Studies, University of Tasmania.

Lawrence LJ (1968) The minerals of the Broken Hill district. *Australasian Institute of Mining and Metallurgy Monograph* **3**, 103–36.

Lawrence LJ and Rafter TA (1962) Sulphur isotope distribution in sulphides and sulphates from Broken Hill South, N.S.W. *Economic Geology* **57**, 217–25.

Leach DL, Sangster DF, Kelley KD, Large RR, Garven G, Allen CR, Gutzmer J and Walters S (2005) Sediment-hosted lead-zinc deposits: a global perspective. *Economic Geology: One Hundredth Anniversary Volume* (eds JW Hedenquist, JFH Thompson, RJ Goldfarb and JP Richards), pp. 561–607. Littleton, Colorado: Society of Economic Geologists.

Lefticariu L, Behum PT, Bender KS and Lefticariu M (2017) Sulfur isotope fractionation as an indicator of biogeochemical processes in an AMD passive bioremediation system. *Minerals* **7**, 41. doi: 10.3390/min7030041.

Li M-L, Liu S-A, Xue C-J and Li D (2019) Zinc, cadmium and sulfur isotope fractionation in a supergiant MVT deposit with bacteria. *Geochimica et Cosmochimica Acta* **265**, 1–19.

Liao S, Tai C, Zhu C, Li H, Li X, Liang J, Yang W and Wang Y (2019) Two episodes of sulfide mineralization at the Yuhuang-1 hydrothermal field on the Southwest Indian Ridge: insight from Zn isotopes. *Chemical Geology* **507**, 54–63.

Liu M-S, Zhang Q, Zhang Y, Zhang Z, Huang F and Yu H-M (2019) High-precision Cd isotope measurements of soil and rock reference materials by MC-ICP-MS with double spike correction. *Geostandards and Geoanalytical Research* **44**, 169–82.

Lockington JA, Cook NJ and Ciobanu CL (2014) Trace and minor elements in sphalerite from metamorphosed sulphide deposits. *Mineralogy and Petrology* **108**, 873–90.

Luck J-M, Othman DB and Albarède F (2005) Zn and Cu isotopic variations in chondrites and iron meteorites: early solar nebula reservoirs and parent-body processes. *Geochimica et Cosmochimica Acta* **22**, 5351–63.

Lydon JW and Reardon NC (2000) Sphalerite compositions of the Sullivan deposit and their implications for its metamorphic history. In *The Geological Environment of the Sullivan Deposit, British Columbia* (eds JW Lydon, T Höy, JF Slack and ME Knapp), pp. 281–301. Geological Association of Canada, Mineral Deposits Division, Special Publication 1.

Maréchal CN, Emmanuel N, Chantal D and Francis A (2000) Abundance of zinc isotopes as a marine biogeochemical tracer. *Geochemistry, Geophysics, Geosystems* **1**, 1–15.

Maréchal CN, Telouk P and Albarède F (1999) Precise analysis of copper and zinc isotopic compositions by plasma-source mass spectrometry. *Chemical Geology* **156**, 251–73.

Marković T, Manzoor S, Humphreys-Williams E, Kirk GJD, Vilar R and Weiss DJ (2017) Experimental determination of zinc isotope fractionation in complexes with the phytosiderophore 2'-deoxymugeneic acid (DMA) and its structural analogues, and implications for plant uptake mechanisms. *Environmental Science & Technology* **51**, 98–107.

Mason TFD, Weiss DJ, Chapman JB, Wilkinson JJ, Tessalina SG, Spiro B, Horstwood MSA, Spratt J and Coles BJ (2005) Zn and Cu isotopic variability in the Alexandrinka volcanic-hosted massive sulphide (VHMS) ore deposit, Urals, Russia. *Chemical Geology* **221**, 170–87.

Matt P, Peck WH, Mathur R, Nurtgen MR and Godfrey L (2022) Zinc isotope constraints on the formation of sedimentary exhalative (SEDEX) ore deposits: New evidence from the Franklin, NJ mining district. *Ore Geology Reviews* **147**, 104970. doi: 10.1016/j.oregeorev.2022.104970.

Matt P, Powell W, Mathur R and deLorraine WF (2020) Zn-isotopic evidence for fluid-assisted ore remobilization at the Balmat Zinc Mine, NY. *Ore Geology Reviews* **116**, 103227. doi: 10.1016/j.oregeorev.2019.103227.

Mavrogenes JA, MacIntosh IW and Ellis DJ (2001) Partial melting of the Broken Hill galena-sphalerite ore; experimental studies in the system PbS-FeS-ZnS-(Ag_2S). *Economic Geology* **96**, 205–10.

Mishra BP, Patia P, Dora ML, Baswani SR, Meshram T, Shareef M, Pattanayak RS, Suryavanshi H, Mishra M and Raza MA (2021) Trace-element systematics and isotopic characteristics of sphalerite-pyrite from volcanogenic massive sulfide deposits of Betul belt, central Indian Tectonic Zone: insight of ore genesis to exploration. *Ore Geology Reviews* **134**, 104149. doi: 10.1016/j.oregeorev.2021.104149.

Nutman AP and Ehlers K (1998) Evidence for multiple Palaeoproterozoic thermal events and magmatism adjacent to the Broken Hill Pb-Zn-Ag orebody, Australia. *Precambrian Research* **90**, 203–38.

O'Brien JJ, Spry PG, Teale GS, Jackson SE and Rogers D (2015) Major and trace element chemistry of gahnite as an exploration guide to Broken Hill-type Pb-Zn-Ag mineralization in the Broken Hill domain, New South Wales, Australia. *Economic Geology* **110**, 1027–57.

Ohmoto H (1972) Systematics of sulfur and carbon isotopes in hydrothermal ore deposits. *Economic Geology* **67**, 557–78.

Page RW and Laing WP (1992) Felsic metavolcanic rocks related to the Broken Hill Pb-Zn-Ag orebody, Australia. Geology, depositional age and timing of high-grade metamorphism. *Economic Geology* **87**, 2138–68.

Page RW, Stevens BPJ and Gibson GM (2005) Geochronology of the sequence hosting the Broken Hill Pb-Zn-Ag orebody. *Economic Geology* **100**, 633–61.

Paniello RC, Day JM and Moynier F (2012) Zinc isotopic evidence for the origin of the Moon. *Nature* **490**, 376–9.

Parr JM (1992) Fluctuations in a magmatic sulphur isotope signature from the Pinnacles mine, New South Wales, Australia. *Mineralium Deposita* **27**, 200–5.

Parr JM (1994a) The geology of the Broken Hill-type Pinnacles Pb-Zn-Ag deposit, western New South Wales, Australia. *Economic Geology* **89**, 778–90.

Parr JM (1994b) The preservation of pre-metamorphic colloform banding in pyrite from the Broken Hill-type Pinnacles deposit, New South Wales, Australia. *Mineralogical Magazine* **58**, 461–71.

Parr JM and Plimer IR (1993) Models for Broken Hill-type lead-zinc-silver deposits. In *Mineral Deposit Modeling* (eds RV Kirkham, WD Sinclair, RI Thorpe and JM Duke), pp. 253–88. Geological Association of Canada Special Paper 40.

Pašava J, Tornos F and Chrastný V (2014) Zinc and sulfur isotope variation in sphalerite from carbonate-hosted zinc deposits, Cantabria, Spain. *Mineralium Deposita* **49**, 797–807.

Peel K, Weiss D, Chapman J, Arnold T and Coles B (2008) A simple combined sample-standard bracketing and inter-element correction procedure for accurate mass bias correction and precise Zn and Cu isotope ratio measurements. *Journal of Analytical Atomic Spectrometry* **23**, 103–10.

Perilya (2008) *Concise Annual Report 2008*. Perth: Perilya Limited, 69 pp.

Phillips GN and Wall VJ (1981) Evaluation of prograde regional metamorphic conditions: their implications for the heat source and water activity during metamorphism in the Willyama Complex. *Bulletin de Mineralogie* **104**, 801–10.

Plimer IR (1979) Sulphide rock zonation and hydrothermal alteration at Broken Hill, Australia. *Transactions of the Institute of Mining and Metallurgy* **88**, B161–76.

Plimer IR (1984) The mineralogical history of the Broken Hill lode, NSW. *Australian Journal of Earth Sciences* **31**, 379–402.

Plimer IR (1985) Broken Hill Pb-Zn-Ag deposit- a product of mantle metasomatism. *Mineralium Deposita* **20**, 147–53.

Pons M-L, Debret B, Bouihol P, Delacour A and Williams H (2016) Zinc isotope evidence for sulfate-rich fluid transfer across subduction zones. *Nature Communications* **7**, 13794. doi: 10.1038/ncomms13794.

Powell T and Downes J (1990) Garnet porphyroblast-bearing leucosomes in metapelites: Mechanisms, phase diagrams, and an example from Broken Hill, Australia. In *High-temperature Metamorphism and Crustal Anataxis* (eds JR Ashworth and M Brown), pp. 105–23. London: Unwin Hyman.

Pratten RD (1965) Lead-silver-zinc ore deposits of the Zinc Corporation and New Broken Hill Consolidated Mines, Broken Hill. In *Geology of Australian Ore Deposits* (ed. J McAndrew), pp. 333–5. 8th Commonwealth Mining and Metallurgy Congress Abstracts. Melbourne: Australasian Institute of Mining and Metallurgy.

Revan MK, Genç Y, Maslennikov VV, Maslennikova SP, Large RR and Danyushevsky LV (2014) Mineralogy and trace-element geochemistry of sulfide minerals in hydrothermal chimneys from the Upper-Cretaceous VMS deposits of the eastern Pontide orogenic belt (NE Turkey). *Ore Geology Reviews* **63**, 129–49.

Ripperger S, Rehkämper M, Porcelli D and Halliday AN (2007) Cadmium isotope fractionation in seawater – a signature of biological activity. *Earth and Planetary Science Letters* **261**, 670–84.

Sangster DF (2020) Evidence that Broken Hill-type Pb-Zn deposits are metamorphosed SEDEX deposits. *Mineralium Deposita* **55**, 1263–70.

Schmitt AD, Galer SJG and Abouchami W (2009) High-precision cadmium stable isotope measurements by double spike thermal ionisation mass spectrometry. *Journal of Analytical Atomic Spectrometry* **24**, 1079–88.

Seedorff E, Dilles JH, Proffett JM, Einaudi MT, Zurcher L, Stavast WJA, Johnson DA and Barton MD (2005) Porphyry deposits: characteristics and origin of hypogene features. *Economic Geology: One Hundredth Anniversary Volume* (eds JW Hedenquist, JFH Thompson, RJ Goldfarb and JP Richards), pp. 251–98. Littleton, Colorado: Society of Economic Geologists.

Spry PG (1987) A sulphur isotope study of the Broken Hill deposit, New South Wales, Australia. *Mineralium Deposita* **22**, 109–15.

Spry PG, McFadden S, Teale GS and Steadman JA (2010) Nodular sillimanite rocks as field indicators of metamorphosed ore deposits: Examples from North America. In *13th Quadrennial International Association on the Geology of Ore Deposits Symposium 2010, Abstracts*, pp. 274–5.

Spry PG, Plimer IR and Teale GS (2008) Did the giant Broken Hill (Australia) Zn-Pb-Ag deposit melt? *Ore Geology Reviews* **34**, 223–41.

Spry PG, Schiller JC and Both RA (1988) Structure and metamorphic setting of base metal mineralisation in the Kanmantoo Group, South Australia. *Bulletin of the Proceedings of the Australasian Institute of Mining and Metallurgy* **293**, 57–65.

Spry PG and Teale GS (2021) A classification of Broken Hill-type deposits: a critical review. *Ore Geology Reviews* **139**, 103935. doi: 10.1016/j.oregeorev.2020.103935.

Spry PG and Wonder JD (1989) Manganoan garnet rich rocks associated with the Broken Hill lead zinc silver deposit, New South Wales, Australia. *Canadian Mineralogist* **27**, 275–92.

Stanton RL and Rafter TA (1966) The isotopic constitution of sulfur in some stratiform lead-zinc ores. *Mineralium Deposita* **1**, 16–29.

Stanton RL and Rafter TA (1967) Sulfur isotope ratios in coexisting galena and sphalerite from Broken Hill, New South Wales. *Economic Geology* **62**, 1088–91.

Strauss H (2004) 4 Ga of seawater evolution: Evidence from the sulfur isotopic composition of sulfate. In *Sulfur Biogeochemistry – Past and Present* (eds JP Amend, KJ Edwards and TW Lyons), pp. 195–205. Geological Society of America Special Paper no. 379.

Teale GS, Groves IM and Manly IM (2006) Mineralisation in the Potosi extended to Flying Doctor area, Northern Leases, Broken Hill. *Geoscience Australia Record* **2006/21**, 182–5.

Telus M, Dauphas N, Moynier F, Tissot FLH, Teng F-Z, Nabelek PI, Craddock PR and Groat LA (2012) Iron, zinc, magnesium and uranium isotopic fractionation during continental crust differentiation: the tale from migmatites, granitoids, and pegmatites. *Geochimica et Cosmochimica Acta* **97**, 247–65.

Toutain J-P, Sonke J, Munoz M, Nonell A, Polvé M, Viers J, Freydier R, Sortino F, Joron J-L and Sumarti S (2008) Evidence for Zn isotopic fractionation at Merapi volcano. *Chemical Geology* **253**, 74–82.

Vokes FM (1976) Caledonian massive sulphide deposits in Scandinavia: a comparative review. In *Handbook of Strata-Bound and Stratiform Ore Deposits, Volume 6* (ed. KH Wolf), pp. 79–128. Amsterdam: Elsevier.

Walters S, Skrzeczynski B, Whiting T, Bunting F and Arnold G (2002) Discovery and geology of the Cannington Ag-Pb-Zn deposit, Mount Isa Eastern Succession, Australia: development and application of an exploration model for Broken Hill-type deposits. In *Integrated Methods for Discovery: Global Exploration in the Twenty-First Century* (eds RJ Goldfarb and RL Nielsen), pp. 95–118. Society of Economic Geologists Special Publication no. 9.

Walters SG (1996) An overview of Broken Hill type deposit. In *New Developments in Broken Hill-Type Deposits* (eds J Pongratz and GJ Davidson), pp. 1–10. CODES Special Publication 1. Hobart: Centre for Ore Deposit and Exploration Studies, University of Tasmania.

Walters SG (1998) Broken Hill-type Pb-Zn-Ag deposits. *Australian Geological Survey Organisation Journal of Australian Geology and Geophysics* **17**, 229–37.

Wang D, Zheng Y, Mathur R, Qiu K, Wu H, Ren H, Wang E, Li Y and Yi J (2021) Zinc and cadmium isotopic constraints on ore formation and mineral exploration in epithermal system: a reconnaissance study at the Keyue and Zhaxikang Sb–Pb–Zn–Ag deposits in southern Tibet. *Ore Geology Reviews* **139**, 104594. doi: 10.1016/j.oregeorev.2021.104594.

Wang D, Zheng Y, Mathur R and Wu S (2018) The Fe-Zn isotopic characteristics and fractionation models: implications for the genesis of the Zhaxikang Sb-Pb-Zn-Ag deposit in southern Tibet. *Geofluids* **18**, 2197891. doi: 10.1155/2018/2197891.

Wang D, Zheng Y, Mathur R and Yu M (2020) Fractionation of cadmium isotope caused by vapour-liquid partitioning in hydrothermal ore-forming system: a case study of the Zhaxikang Sb–Pb–Zn–Ag deposit in Southern Tibet. *Ore Geology Reviews* **119**, 103400. doi: 10.1016/j.oregeorev.2020.103400.

Wasylenki LE, Swihart JW and Romaniello SJ (2014) Cadmium isotope fractionation during adsorption to Mn oxyhydroxide at low and high ionic strength. *Geochimica et Cosmochimica Acta* **140**, 212–26.

Webster AE (2006) *The Geology of the Broken Hill Lead-Zinc-Silver Deposit, New South Wales, Australia*. CODES ARC Centre of Excellence in Ore Deposits Monograph 1. Hobart: ARC Centre of Excellence in Ore Deposits, University of Tasmania, 278 pp.

Wen H, Zhu C, Zhang Y, Cloquet C, Fan H and Fu S (2016) Zn/Cd ratios and cadmium isotope evidence for the classification of lead-zinc deposits. *Nature Scientific Reports* **6**, 25273. doi: 10.1038/srep25273.

White RW, Powell R and Halpin JA (2004) Spatially-focused melt formation in aluminous metapelites from Broken Hill, Australia. *Journal of Metamorphic Geology* **22**, 825–45.

Whitney DL and Evans BW (2010) Abbreviations for names of rock-forming minerals. *American Mineralogist* **95**, 185–7.

Widdop WG (1983) The geology of the Fitzpatrick area, North Broken Hill Limited, Broken Hill, NSW. In *Broken Hill Conference, 1983: The Australasian Institute of Mining Metallurgy Proceedings*, pp. 177–82. Parkville: Australasian Institute of Mining and Metallurgy.

Wilkinson JJ, Weiss DJ, Mason TFD and Coles BJ (2005) Zinc isotope variation in hydrothermal systems: preliminary evidence from the Irish Midlands ore field. *Economic Geology* **100**, 583–90.

Williams PJ, Chapman LH, Richmond J, Baker T, Heinemann M and Pendergrast WJ (1996) Significance of late orogenic metasomatism in the Broken Hill-type deposits of the Cloncurry district, NW Queensland. In *New Developments in Broken Hill-Type Deposits* (eds J Pongratz and GJ Davidson), pp. 119–32. CODES Special Publication 1. Hobart: Centre for Ore Deposit and Exploration Studies, University of Tasmania.

Williams-Jones AE and Heinrich CA (2005) Vapor transport of metals and the formation of magmatic-hydrothermal ore deposits. *Economic Geology* **100**, 1287–312.

Willis IL, Brown RE, Stroud WJ and Stevens BPJ (1983) The early Proterozoic Willyama Supergroup: stratigraphic subdivision and interpretation of high to low-grade metamorphic rocks in the Broken Hill Block, New South Wales. *Journal of the Geological Society of Australia* **30**, 195–224.

Wohmbacher F, Rehkämper M and Mezger K (2004) Determination of the mass dependence of cadmium isotope fractionation during evaporation. *Geochimica et Cosmochimica Acta* **68**, 2349–57.

Wohmbacher F, Rehkämper M, Mezger K, Bischoff A and Münker C (2008) Cadmium stable isotope cosmochemistry. *Geochimica et Cosmochimica Acta* **72**, 646–67.

Wohmbacher F, Rehkämper M, Mezger K and Münker C (2003) Stable isotope compositions of cadmium in geological materials and meteorites

determined by multi-collector ICPMS. *Geochimica et Cosmochimica Acta* **67**, 4639–54.

Wright JV, Haydon RC and McConachy GW (1987) Sedimentary model for the giant Broken Hill Pb-Zn deposit, Australia. *Geology* **15**, 598–602.

Wu T, Huang Z, He Y, Yang M, Fan H, Wei C, Ye L, Hu Y, Xiang Z and Lai C (2021) Metal source and ore-forming process of the Maoping carbonate-hosted Pb-Zn deposit in Yunnan, SW China: evidence from deposit geology and sphalerite Pb-Zn-Cd isotopes. *Ore Geology Reviews* **135**, 104214. doi: 10.1016/j.oregeorev.2021.104214.

Xu C, Zhong H, Hu R-Z, Wen H-J, Zhu W-G, Bai Z-J, Fan H-F, Li F-F and Zhou T (2020) Sources and ore-forming fluid pathway of carbonate-hosted Pb-Zn deposits in Southwest China: implications of Pb-Zn-S-Cd isotopic compositions. *Mineralium Deposita* **55**, 491–513.

Xu L-J, Liu S-A and Li S (2021) Zinc isotopic behavior of mafic rocks during continental deep subduction. *Geoscience Frontiers* **12**, 101182. doi: 10.1016/j.gsf.2021.101182.

Xuesin S (1984) Minor elements and ore genesis of the Fankou lead-zinc district. *Mineralium Deposita* **19**, 95–104.

Yang Z, Song W, Wen H, Zhang Y, Fan H, Wang F, Li Q, Yang T, Zhou Z, Liao S and Zhu C (2022) Zinc, cadmium and sulphur isotopic compositions reveal biological activity during formation of a volcanic-hosted massive sulphide deposit. *Gondwana Research* **101**, 103–13.

Zhao Y, Vance D, Abouchami W and de Baar HJW (2014) Biogeochemical cycling of zinc and its isotopes in the Southern Ocean. *Geochimica et Cosmochimica Acta* **125**, 653–72.

Zhou J-X, Huang Z-L, Lv Z-C, Zhu X-K, Gao J-G and Mirnejad H (2014a) Geology, isotope geochemistry and ore genesis of the Shanshulin carbonate-hosted Pb–Zn deposit, southwest China. *Ore Geology Reviews* **63**, 209–25.

Zhou J-X, Huang Z-L, Zhou M-F, Zhu, A-K and Muchez P (2014b) Zinc, sulfur and lead isotopic variations in carbonate-hosted Pb-Zn sulfide deposits, southwest China. *Ore Geology Reviews* **58**, 41–54.

Zhu C, Liao S, Wang W, Zhang Y, Yang T, Fan H and Wen H (2018) Variations in Zn and S isotope chemistry of sedimentary sphalerite, Wusihe Zn-Pb deposit, Sichuan Province, China. *Ore Geology Reviews* **95**, 639–48.

Zhu C, Wen H, Zhang Y and Fan H (2016) Cadmium and sulfur isotopic compositions of the Tianbaoshan Zn-Pb-Cu deposit, Sichuan Province, China. *Ore Geology Reviews* **76**, 152–62.

Zhu CW, Wen H, Zhang Y-X, Fan H-F, Fe S-H, Xu J and Qin T-R (2013) Characteristics of Cd isotopic compositions and their genetic significance in the lead-zinc deposits of SW China. *Science China–Earth Sciences* **56**, 2056–65.

Zhu C, Wen H, Zhang Y, Huang Z, Cloquet C, Luais B, and Yang T (2021) Cadmium isotopic constraints on metal sources in the Huize Zn–Pb deposit, SW China. *Geoscience Frontiers* **12**, 101241. doi: 10.1016/j.gsf.2021.101241.